



ORIGINAL RESEARCH ARTICLE

Advanced Manufacturing of Titanium Alloy Ti-6Al-4V by Combining Cryogenic Machining and Ultrasonic-Assisted Turning

Roland Bejjani , Elie Bachir, and Charlie Salame

Submitted: 6 March 2023 / Revised: 6 June 2023 / Accepted: 11 June 2023 / Published online: 30 June 2023

Cryogenic and ultrasonic-assisted turning have both beneficial effects on the machinability of difficult-to-machine materials, such as titanium alloy Ti-6Al-4V. This research investigates the effect of combining both cryogenic and ultrasonic-assisted machining, to assess the effects on cutting temperature, forces and tool wear. The research utilizes FEM and CFD models to provide a better understanding of the interaction between the mechanisms at work during the machining process—namely the ultrasonic motion of the tool and the cryogenic impingement of the tool. The experimentation is then conducted to prove the effectiveness of combining both methods in reducing the cutting forces and reducing tool wear. The combined process is compared to conventional turning, cryogenic turning and ultrasonic-assisted turning. The CFD and FEM results showed a decrease in tool and chip temperature by 7.26% and 13.86%, respectively, when compared to UAT. The cutting forces in the combined turning show a reduction of 22% when compared to conventional turning. Tool wear is analyzed for the 4 cases. Tool wear caused by adhesion is shown to decrease in the new combined cutting method. This research has scientific as well as potential industrial applications in the machining of difficult-to-machine materials.

Keywords cryogenic, machining, titanium, tool wear, ultrasonic

1. Introduction

The machinability of difficult-to-machine materials has long posed a challenge for manufacturers, where the increase in productivity is often accompanied by adverse effects on their machinability. Titanium alloys, such as Ti-6Al-4V, are notorious for their challenging machinability, attributed to the very high cutting temperatures which lead to premature tool wear and decrease in the surface quality of the machined workpiece (Ref 1). Specifically, the low thermal conductivity of Ti64 and the high reactivity between the tool and workpiece material help accelerate tool wear, which negatively affects the productivity of the alloy and the quality of the workpiece (Ref 2).

The introduction of advanced manufacturing methods such as cryogenic machining (CM) and ultrasonic-assisted turning (UAT) showed improvements in the machinability of these materials (Ref 3). Zhang and Wang (Ref 4) developed a 2D finite element model (FEM) to compare the effective stresses in turning Ti64 and noticed a decrease of 50% when comparing UAT to conventional machining. Patil et al. (Ref 5) showed a reduction of up to 43% in cutting forces due to the ultrasonic motion of the cutting tool when machining Ti-6Al-4V. UAT has

List of Symbols

k	Kinetic energy
ε	Turbulence energy
ρ	Density
μ	Molecular viscosity
σ_k	Turbulence Prandtl number
G_k	Turbulence kinetic energy due to the mean velocity gradients
G_b	Turbulence kinetic energy due to the mean velocity buoyancy
S_{ij}	Mean strain rate
η	Effectiveness factor
ν	Kinematic viscosity
σ_ε - σ_k	Turbulent Prandtl numbers
S_ε	Source term
α_q	Phase- q volume fraction
ρ_q	Phase density
\dot{m}_{pq}	Mass transferred from phase p to q
\dot{m}_{qp}	Mass transferred from phase q to p
$S_{\alpha q}$	Mass source term
$x(t)$	Instantaneous tool displacement
X_0	Amplitude of vibrations
f	Frequency
$\bar{\sigma}$	Johnson–Cook flow stress
A	Initial yield stress
B	Hardening modulus
C	Strain rate factor
n	Work hardening exponent
m	Thermal softening coefficient
α	Strain rate for Johnson–Cook equation

Roland Bejjani and Elie Bachir, Lebanese American University, Byblos, Lebanon; and Charlie Salame, Chalmers University of Technology, Gothenburg, Sweden. Contact e-mail: rolandbejj@gmail.com.

List of Symbols	
β	Reference strain rate
T_{melt}	Melting temperature
T_{room}	Room temperature
w	Damage parameter
$\Delta\bar{\epsilon}^{\text{pl}}$	Equivalent plastic strain
$\bar{\epsilon}_f^{\text{pl}}$	Failure strain
$\epsilon^{\text{pl}}/\dot{\epsilon}_0$	Nondimensional plastic strain rate
q	Pressure stress
p	Mises stress
D_1 - D_5	Damage constants
$\dot{\epsilon}_0$	Reference strain rate

also been shown to increase the cutting temperature by 50% due to the addition of energy into the cutting process (Ref 6). The addition of an external source of heat further increases the cutting temperature while reducing the cutting forces which would increase the tool wear and reduce the tool life (Ref 7). Research on UAT suggests that adding a coolant to the process might enhance the cutting process by reducing the cutting forces and reducing tool wear (Ref 8).

Previous work also showed important improvements when cryogenically machining titanium alloys compared to dry cutting. Cryogenic turning performed by Jerold and Kumar led to a temperature decrease of up to 50% when compared to dry turning of Ti-6Al-4V (Ref 9). When cryogenically milling Ti64, Sadik and Isakson measured a 6-time increase in tool life for the case of cryogenic machining compared to dry milling (Ref 10). In terms of tool wear, adhesive wear was shown to decrease under cryogenic application compared to dry turning of Ti64 (Ref 11). The surface roughness of the Ti64 workpiece was also shown to be affected by the cryogenic application, with a 19% decrease in surface roughness when cryogenically machining Ti64 compared to dry machining (Ref 12). Airao et al. (Ref 13) found that when UAT and CM are combined tool wear was reduced.

Available literature has discussed the beneficial effects of CM and UAT independently, but the effect of combining both advanced machining methods together is still not clear. This research aims to address this gap in the literature and study the effect of combining CM and UAT on the cutting temperatures, cutting forces and tool wear during the turning of Ti64. The research utilizes simulation and experimental data to compare conventional turning to cryogenic, ultrasonic assisted and combined turning. The simulation part involves the use of finite element (FEM) and computational fluid dynamics (CFD) models that model the orthogonal cutting of the Ti64 workpiece under different cutting conditions to compare forces and temperature profiles of the cutting process. The simulation was used to better understand the mechanisms involved in the process and to identify the parameters to be used experimentally. The convection coefficient is retrieved from the CFD model and used as film coefficient in the FEM model. Experiments were conducted and the resulting tool wear was analyzed taking into consideration the FEM results as shown in Fig. 1.

The research provides a better understanding of the combined effect of CM and UAT, using the thermo-fluid properties of the fluid from CFD and using it to better understand the obtained simulation and experimental results

The work also analyzes the tool wear mechanisms and the effect of each advanced method independently, as well as the combined method, to be compared to the tool wear observed in the conventional turning of Ti64. Lastly, the study also promotes industrial implications, where the joint method of combining CM and UAT could provide an industrial solution that reduces cutting forces and tool wear, subsequently increasing the productivity of these alloys.

2. CFD and FEM Models

2.1 CFD Model

The CFD model was used to simulate the cryogenic impingement near the cutting zone, in order to obtain the cutting temperatures, convection coefficients and thermo-fluid properties near the tool–chip interface. The difficulty in obtaining the experimental 3D temperature profiles near the tool–chip interface, as well as the convection coefficients and thermo-fluid properties, necessitated the use of a CFD model to simulate the cryogenic environment. This would enhance the understanding of the cryogenic effect on the machining, for both the cryogenic and combined cutting experiment.

Two CFD models were used to simulate the cryogenic impingement on the tool–chip interface—the first model simulated the cryogenic case alone while the other modeled the combined (UAT and CM) tool–chip geometry. The two models were identical to each other except for the addition of a separation gap between the tool and chip in the combined model, to account for the tool’s separation from the workpiece because of its vibrating motion.

The nonlinear nature of the flow, especially near the cutting zone, makes the CFD results essential to understand the cryogenic environment and help understand the experimental results for the cryogenic and combined experiments. Since experimentally obtaining the 3D temperature profile, evaporation rates profile and convection coefficients are extremely difficult, the CFD model is used to provide these values.

The CFD model compares the temperature distribution with gap versus no gap to see the effect of the ultrasonic vibration on the cryogenic cooling near the cutting zone. The results are then fed back to the FEM model to simulate the cryogenic and combined cutting of the titanium alloy. In the combined FEM simulation, the gap, when existing, between the tool and workpiece is modeled using the convection coefficients obtained from the CFD simulation. This allows for a more accurate simulation of the combined effect between cryogenic and ultrasonic-assisted turning.

2.1.1 Geometry and Setup. The setup for the CFD model is shown in Fig. 2. Carbon dioxide is delivered to the tool–chip interface through a nozzle. The tool is vibrating along the cutting direction as shown in Fig. 2. The area of interest is simulated using a CFD model. The setup is further explained in Sect. 3.2.

The two CFD models have a similar geometry, except for the existence of a separation gap in the combined simulation. Figure 3 shows the setup for the CFD simulations. The width of the gap is set to be identical to the experimental setup to allow an accurate simulation of the cryogenic impingement. The geometry of the setups, along with the boundary conditions, is shown in Fig. 3. Cryogenic fluid is carbon dioxide. The inlet is

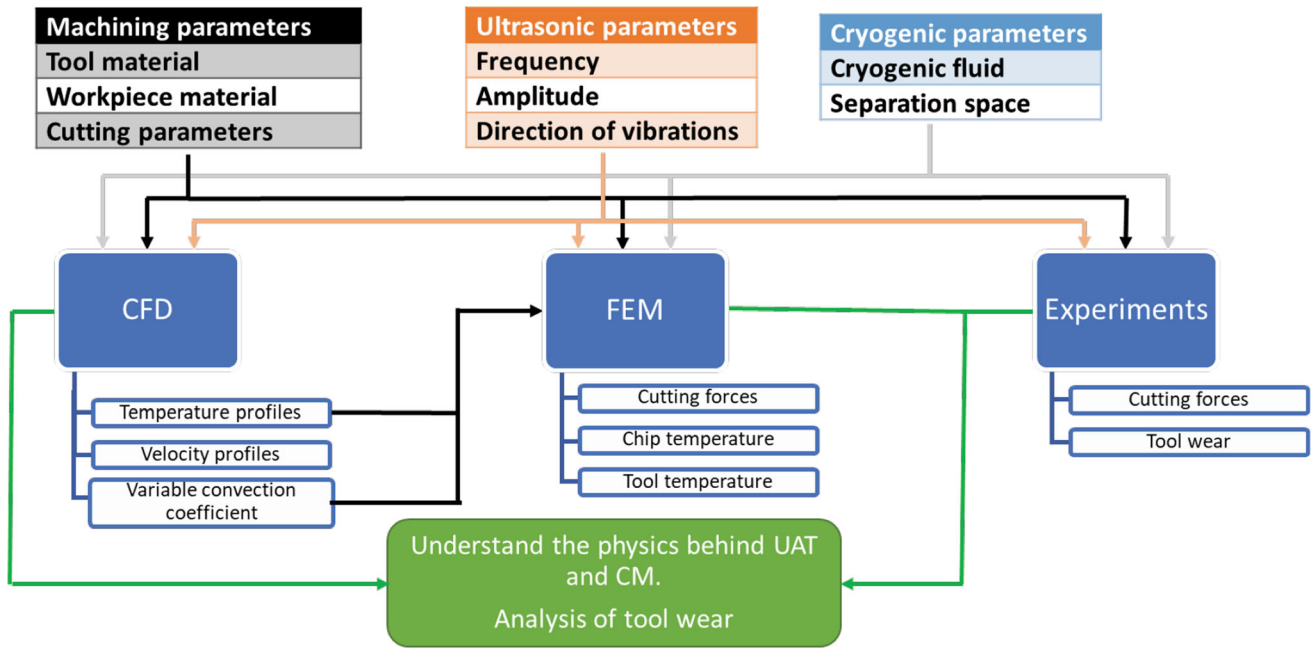


Figure 1 Methodology flowchart

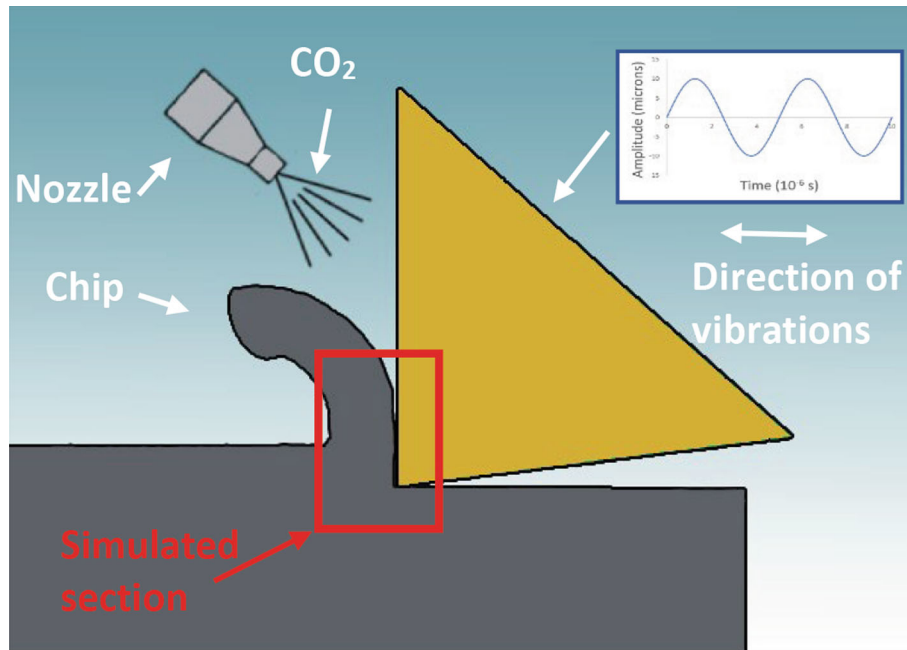


Figure 2 Setup for the computational fluid dynamics simulations

set to have a pressure inlet at 8 bars, with the cryogenic fluid assumed 100% liquid. The outlet is a pressure outlet at atmospheric pressure, while the tool and chip are set as coupled walls to allow the heat transfer between the mediums.

The initial temperature profiles for the CFD geometry were obtained from the conventional cutting simulation, and then inserted into MATLAB using a developed subroutine to yield a distribution function for the geometry temperature. This was done by using multiple nodes' spatial coordinates (x_i, y_i) to have a system of points and their equivalent temperatures (x_i, y_i, T_i). These points were then inputted to MATLAB as vectors to yield a polynomial surface fit of third degree in x and y , with a

high goodness of fit (greater than 97% for all cases). Once the functions were obtained, they were used during hybrid initialization of the CFD model in function of x and y , while the temperature in the z -direction was initially set as constant. This process was applied to the chip, tool, and workpiece.

The heat generation rates in the primary and secondary shear zones were obtained from the conventional cutting FEM simulation and inserted to the CFD simulations to account for the dynamic nature of the heat transfer during machining. The heat generation was assumed to be constant throughout the simulation time, and the heat generation rate in the tertiary shear zone was assumed negligible (Ref 14). Heat transfer is

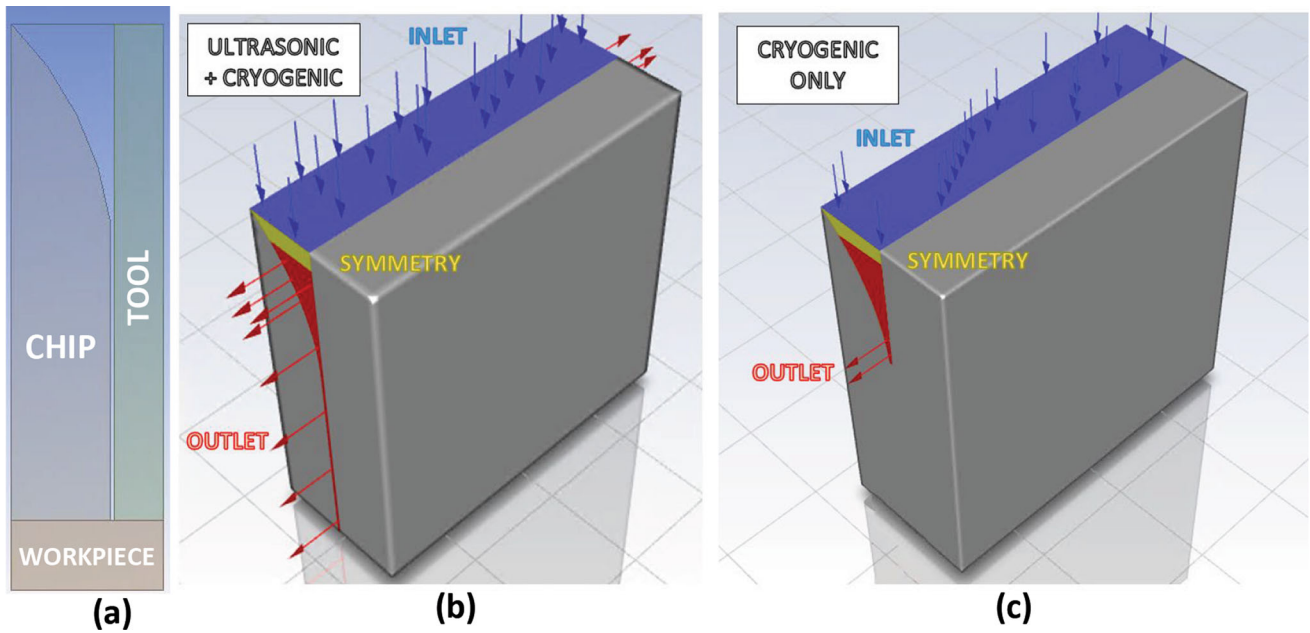


Figure 3 (a) Cross section of the geometry showing the chip, tool and workpiece (b) Boundary conditions for the simulation with the gap (combined simulation) and (c) Boundary conditions for the simulation without the gap (cryogenic only)

activated by conduction and the heat is allowed to propagate in all directions between the different solids, given the use of coupled walls as boundary conditions for the solid media.

Heat convection is also considered in the model, allowing for heat exchange between the impinging cryogen and the tool–workpiece geometry. The inlet is assumed to have a liquid volume fraction of 1.0. The fluid then undergoes evaporation due to the change in pressure and temperature, according to the temperature–pressure saturation curve. The fluid absorbs heat from the tool–chip geometry, which is at a considerably higher temperature. When the liquid particles have absorbed the equivalent to the latent heat of vaporization, they evaporate. As discussed in the results of the CFD simulations in Sect. 4.1, the evaporation rates vary from point to point, thus affecting the convection coefficient at the different locations near the tool–chip interface.

2.1.2 Governing Equations. The continuity, momentum and energy equations constitute the general equations that dictate fluid dynamics. Specific to this model, the multiphase model is chosen to be the volume of fluid and the turbulence model is selected to be the k -epsilon turbulence model (realizable).

Turbulence model: Realizable k -Epsilon

The realizable k -Epsilon computes 2 equations: the equation for turbulence kinetic energy k and that for dissipation of turbulence energy ϵ , shown in Eq. 1 and 2, respectively (Ref 15–17),

$$\frac{\partial}{\partial t}(\rho k) + \frac{\partial}{\partial x_j}(\rho k u_j) = \frac{\partial}{\partial x_j} \left[\left(\mu + \frac{\mu_t}{\sigma_k} \right) \frac{\partial k}{\partial x_j} \right] + G_k + G_b - \rho \epsilon - Y_M + S_k \quad (\text{Eq 1})$$

where ρ is the density, μ is the molecular viscosity, u_j is the velocity projection in the corresponding direction, and σ_k is the turbulent Prandtl number. G_k and G_b are turbulence kinetic energies due to the mean velocity gradients and buoyancy, and

S_k is a source term. Y_M represents the fluctuating dilatation in compressible turbulence to the overall dissipation rate.

$$\frac{\partial}{\partial t}(\rho \epsilon) + \frac{\partial}{\partial x_j}(\rho \epsilon u_j) = \frac{\partial}{\partial x_j} \left[\left(\mu + \frac{\mu_t}{\sigma_\epsilon} \right) \frac{\partial \epsilon}{\partial x_j} \right] + \rho C_1 S_\epsilon - \rho C_2 \frac{\epsilon^2}{k + \sqrt{\nu \epsilon}} + C_{1\epsilon} \frac{\epsilon}{k} C_{3\epsilon} G_b + S_\epsilon \quad (\text{Eq 2})$$

where $C_1 = \max \left[0.43, \frac{\eta}{\eta+5} \right]$, $\eta = S \frac{k}{\nu}$, $S = S_{ij} \sqrt{2}$, S_{ij} is the mean strain rate, η is the effectiveness factor, ν is the kinematic viscosity, C_2 and $C_{1\epsilon}$ are constants, σ_ϵ and σ_k are the turbulent Prandtl numbers, and S_ϵ is a source term.

Multiphase model: Volume of fluid (VoF)

The VoF model solves a volume fraction continuity equation for each secondary phase in the system, shown in Eq. 3 (Ref 15). For the primary phase, ANSYS calculates the volume fraction based on the condition that the sum of all phases should amount to 1. The equations are solved by an explicit time discretization with implicit body forces.

$$\frac{1}{\rho_q} \left[\frac{\partial}{\partial t}(\alpha_q \rho_q) + \nabla \cdot (\alpha_q \rho_q \vec{v}_q) \right] = S_{\alpha q} + \sum_{p=1}^n (\dot{m}_{pq} - \dot{m}_{qp}) \quad (\text{Eq 3})$$

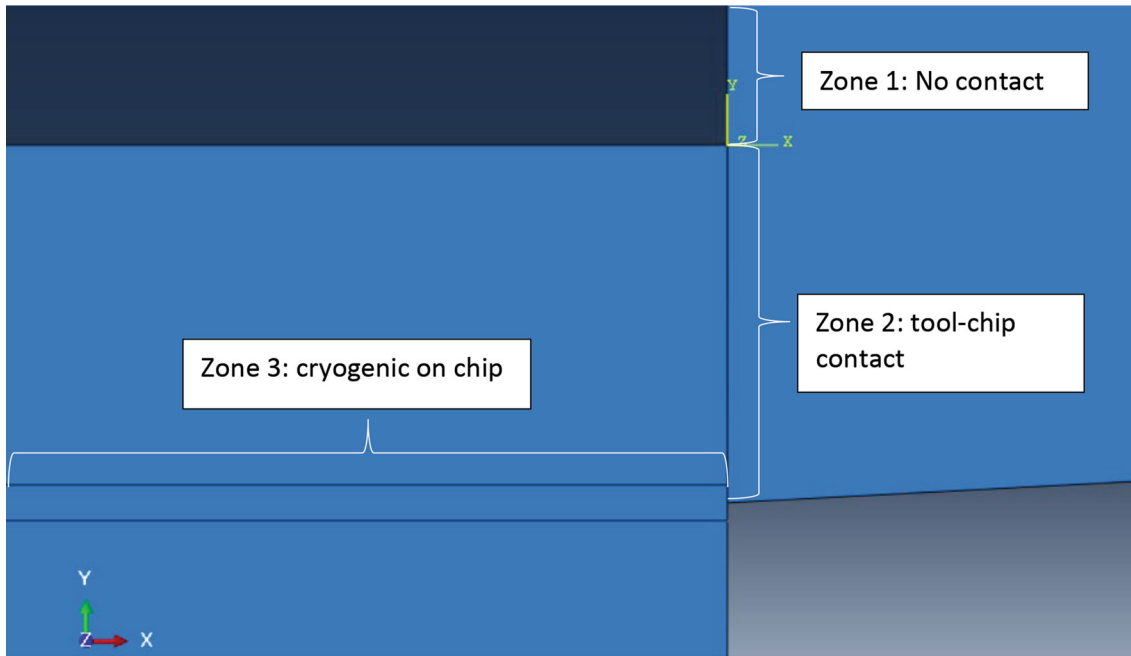
where α_q is the phase- q volume fraction, ρ_q is the phase's density, \dot{m}_{pq} is the mass transferred from phase p to phase q and \dot{m}_{qp} from phase q to p . The mass source term $S_{\alpha q}$ is zero.

2.2 FEM Model

2.2.1 Geometry, Meshing and Setup. The main objective of the FEM study is to have a range of temperature on the cutting tool to compare the different cutting methods. For that end, we used a validated 2D model to save on processing

Table 1 Material properties for workpiece and tool

Parameter	Young's modulus, GPa	Poisson's ratio	Specific heat, J/kg °C	Thermal conductivity, W/m °C	Density, kg/m ³	Friction coefficient
Workpiece (Ti-6Al-4V)	119	0.33	570	7.3	4512	0.3
Tool (W-C)	686	0.22	197	162	15800	

**Figure 4** Application zones of the cryogenic fluid in FEM

resources. The FEM was performed in 2D due to the limitation in computing capacity for a 3D model of this complexity. The ultrasonic and cryogenic conditions were added to the model to simulate UAT, CM and the combined method. The material of the workpiece and tool are summarized in Table 1 (Ref 16). A sharp tool was used. The rake angle used in the model and the clearance angle are 0° and 7° , respectively.

The workpiece was given a constant linear velocity in the cutting direction and was fixed for rotation and vertically. The tool was defined as a solid body. For the dry cutting simulations, the tool was fixed in all directions. For the simulations containing ultrasonic vibrations, the tool was given in the cutting direction a periodic motion following the path described in Eq. 4,

$$x(t) = X_0 \sin(2\pi ft) \quad (\text{Eq 4})$$

where X_0 is the amplitude of the vibration. The amplitude was given the value of 10 microns for a maximum total displacement of 20 microns for the tool from + 10 to – 10 microns. The ultrasonic device was given the appropriate signal to provide the same displacement of 20 microns in the experiments. The frequency f was defined as 20 KHz to match the experiments.

The workpiece was defined as a deformable body, while the tool was defined as a solid since wear was not included in the simulation and the effect of the ultrasonic and cryogenic

turning on tool temperature was studied. The initial temperature of the tool and the workpiece was set at 25°C and the effect of the convection of the environment was included. A simple Coulomb friction of 0.3 was assumed in the simulations for the surface-to-surface interaction between tool and workpiece (Ref 16). The meshing element CPE4RT was used with a thermo-coupled dynamic explicit analysis (Ref 18), where conduction between the tool and the workpiece is applied in addition to conduction within the tool.

The cryogenic fluid in the finite element model was accounted for by dividing the areas where the cryogenic fluid is applied into 3 separate zones as shown in Fig. 4. A space- and time-dependent film (or convection) coefficient was retrieved from the CFD simulation and was added on each zone separately for a realistic simulation of the cooling effect of the cryogenic fluid.

The first zone is defined as the zone where there is no contact between the tool and the workpiece/chip, shown in Fig. 4. The cooling effect is not interrupted on this zone since no material is blocking the cryogenic fluid. Therefore, the convection coefficient used from the CFD was continuously applied on this area at every time step.

The second zone is the tool–chip contact zone where intermitted cooling is applied. The cryogenic fluid is interrupted from reaching the area during the cutting process due to the contact between the tool and the chip. The separation duration

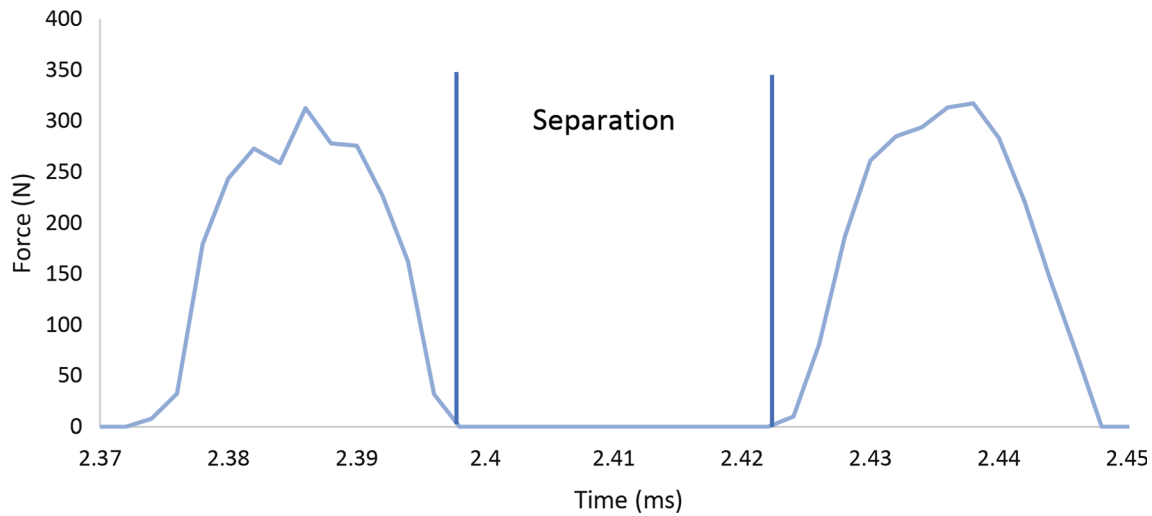


Figure 5 Separation from ultrasonic-assisted turning finite element model

Table 2 Johnson–Cook material and damage model values for titanium alloy

Parameter	A	B	C	n	m
Value	782.7 MPa	498.4 MPa	0.028	0.28	1
Parameter	$D1$	$D2$	$D3$	$D4$	$D5$
Value	− 0.09	0.25	− 0.5	0.014	3.87

was retrieved from the cutting forces output of the simulation where only UAT is applied. The absence of cutting forces was selected as the duration at which separation is present, as shown in Fig. 5. The time instances were tabulated and inserted as a table defined time amplitude in the study to enable and disable the cryogenic application to this tool–chip contact zone. During the separation, the convection coefficient values, which are dependent on the location along the tool at the tool–chip interface, are added to the second zone and removed completely when the tool is in contact with the workpiece.

Finally, the third zone is along the chip. Cryogenic fluid is applied on the to-be-formed chip in the model. The convection coefficient was applied on the third zone as the cutting process progressed. The cooling effect was disabled initially and enabled on the mesh nodes along the depth of cut only when the chip is starting to form.

Four simulations were developed, where conventional turning, ultrasonic turning, cryogenic turning and the combined method are studied. The cutting speed selected was 7.2 m/min since the ultrasonic effect and separation are mostly effective at low cutting speeds. The depth of cut is 0.1 mm to simulate a finishing process with a low depth of cut, matching the experimental work.

2.2.2 Material and damage models. For the FEM section of this study, the Johnson–Cook and damage model was followed to simulate the chip formation and separation process. Equation 5 was used for the Johnson–Cook model (Ref 16):

$$\bar{\sigma} = [A + B(\bar{\epsilon})^n] \left[1 + C \ln\left(\frac{\dot{\alpha}}{\beta}\right) \right] \left[1 - \left(\frac{T - T_{\text{room}}}{T_{\text{melt}} - T_{\text{room}}} \right)^m \right] \quad (\text{Eq 5})$$

where in Eq. 5, A is the initial yield, B is the hardening modulus and C is the strain factor. Also, n stands for the work hardening exponent, m is the thermal softening coefficient. The reference strain rate used to normalize the strain rate α is $\beta=1$. The melting temperature of the material is defined as T_{melt} and the room temperature as T_{room} . The properties of the titanium alloy used in this study are summarized in Table 2 (Ref 19).

The fracture criteria selected in this study are the Johnson–Cook damage criterion to simulate the fracture of the titanium workpiece and initiate the formation of the chip. Fracture is initiated when the damage parameter exceeds the value of 1 and the elements are deleted. Equation 6 describes the damage parameter:

$$w = \sum \left(\frac{\Delta \bar{\epsilon}^{\text{pl}}}{\bar{\epsilon}_f^{\text{pl}}} \right) \quad (\text{Eq 6})$$

where $\Delta \bar{\epsilon}^{\text{pl}}$ and $\bar{\epsilon}_f^{\text{pl}}$ are the increment of equivalent plastic strain and the failure strain, respectively. The failure strain, $\bar{\epsilon}_f^{\text{pl}}$ is dependent on multiple parameters which are a nondimensional plastic strain rate $\dot{\epsilon}^{\text{pl}}/\dot{\epsilon}_0$ and a one dimensionless pressure/deviatoric stress ratio p/q (where p is the pressure stress and q is the Mises stress). The following equation describes the damage (Ref 20):

$$\bar{\epsilon}_f^{\text{pl}} = \left[D_1 + D_2 \exp\left(D_3 \frac{p}{q}\right) \right] \left[1 + D_4 \ln\left(\frac{\dot{\epsilon}^{\text{pl}}}{\dot{\epsilon}_0}\right) \right] (1 + D_5 T^*) \quad (\text{Eq 7})$$

$$T^* = \frac{T - T_r}{T_m - T_r} \quad (\text{Eq 8})$$

where D_1 – D_5 are damage constants, $\dot{\epsilon}_0$ is the reference strain rate and ϵ^{pl} is the failure strain. T_m is the melting temperature of the material and T_r is the room temperature. The damage criterion constants for titanium alloys are summarized in Table 2 (Ref 19, 20).

3. Experiments

Longitudinal turning experiments were conducted in addition to the FEM simulations for a better understanding of the effect of combining cryogenic machining and ultrasonic-assisted turning. The experiments were longitudinal turning to enable a longer cutting path without interruption for the study of wear. Longitudinal turning was also selected for the experiments for the nozzle to follow exactly the tool holder at a constant angle without affecting the convection coefficient.

3.1 Design of Experiments

The selection of parameters for the experimental work was based on the previously determined depth of cut, feed and cutting speed for the simulations which were selected for the greatest effect of the combined work of UAT and cryogenic machining. The low depth of cut, feed and cutting speed were chosen in a way where actual tool-workpiece separation was perceived to integrate the cryogenic fluid into the tool-chip interface.

Four total experiments were conducted as shown in Table 3. The experiments were for dry cutting (conventional turning), ultrasonic-assisted turning, cryogenic machining and the combined method. A calculation using the kinematics of motion of tool vibration and workpiece was conducted to determine a range of speed to guarantee the presence of separation. The separation occurs when the cutting speed is lower than the instantaneous speed of the tool that was derived from Eq. 4. The selected feed was 0.1 mm/rev, the depth of cut 0.1 mm and the cutting speed 7.2 m/min.

Tool geometry matched the geometry of the tool used in the simulation. As shown in Table 3, the tool used is a CNMG

Table 3 Design of experiments

	Cryogenic application	Vibration addition	Cutting time
1	No	No	3 min
2	No	Yes	
3	Yes	No	
4	Yes	Yes	

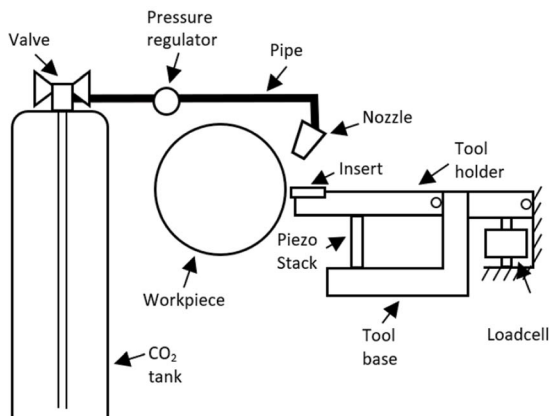


Figure 6 Experimental setup

carbide tool with a TiAlN coating. The workpiece selected is a solid bar of Ti-6Al-4V with a diameter of 100 mm.

3.2 Experimental Setup

The experimental setup shown in Fig. 6 shows the cryogenic system and the ultrasonic system. The cutting forces were retrieved by a special tool design where the tool holder was fixed on a pin and the cutting forces were measured on a tension load cell to eliminate the effect of the forces added externally by the piezoelectric induced vibrations. The forces caused by the added vibration were introduced as internal forces to the tool design so that only the forces resulting from cutting were registered. An external cryogenic system was used to deliver the cryogenic fluid to the tool-chip interface for the cryogenic and combined experiments. The cryogenic system consisted of a converging nozzle, insulated pipe, pressure regulator and pressurized tank. The system supplies carbon dioxide at a pressure of 8 bars through the 1-mm exit diameter of the converging nozzle. Scanning electron microscope (SEM) and energy-dispersive spectroscopy (EDS) analysis was conducted on the COXEM SEM machine to analyze tool wear.

4. Results and Discussion

4.1 Simulation Results and Discussion

CFD simulations were conducted first to retrieve the convection coefficients during cryogenic cutting and to use the values as input in the FEM model. The model was also used to explain the effect of the presence of separation on the cryogenic machining. The results of the simulations are presented below.

4.1.1 CFD Results. The CFD simulations yielded the temperature profiles, velocity profiles and the heat convection coefficients, as shown in Fig. 7, 8 and 9, respectively. As shown in Fig. 7, there is a noticeable difference between the cooling of the tool in the combined versus the cryogenic-only simulation. The tool in the cryogenic-only simulation exhibits a higher temperature of 750 K than the one in the combined machining which was 620 K. This can be attributed to the enhanced penetration of the cryogenic fluid caused by the ultrasonic motion of the tool, leading to separation of the tool from the



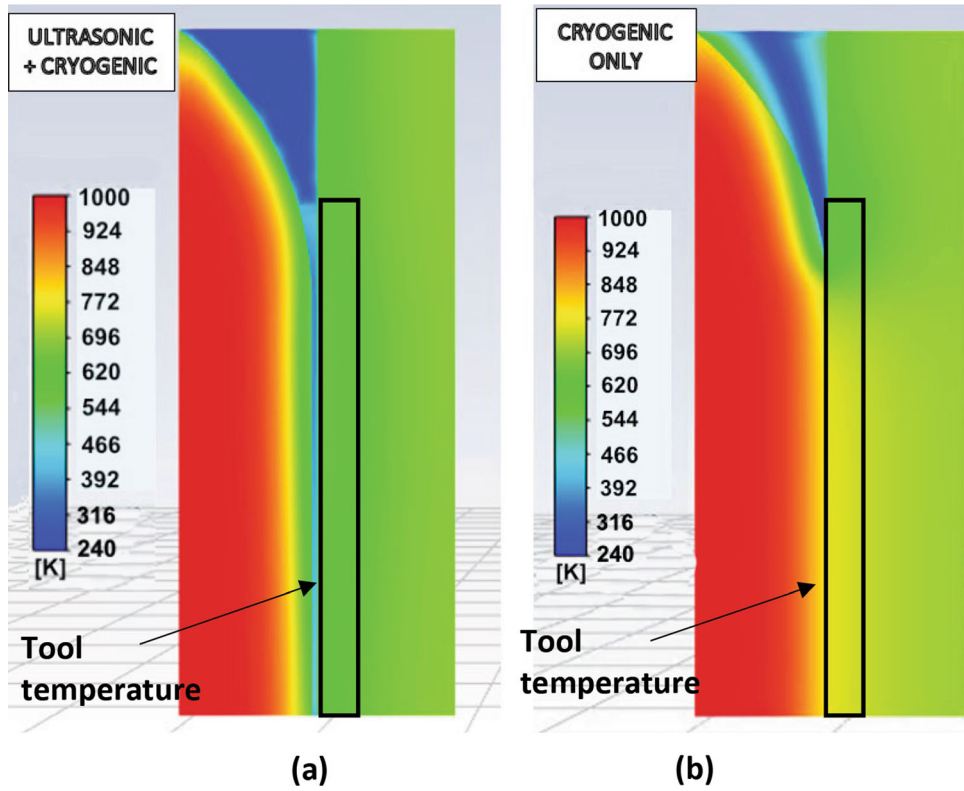


Figure 7 Temperature profiles of the tool–chip geometry for (a) combined machining and (b) cryogenic-only machining

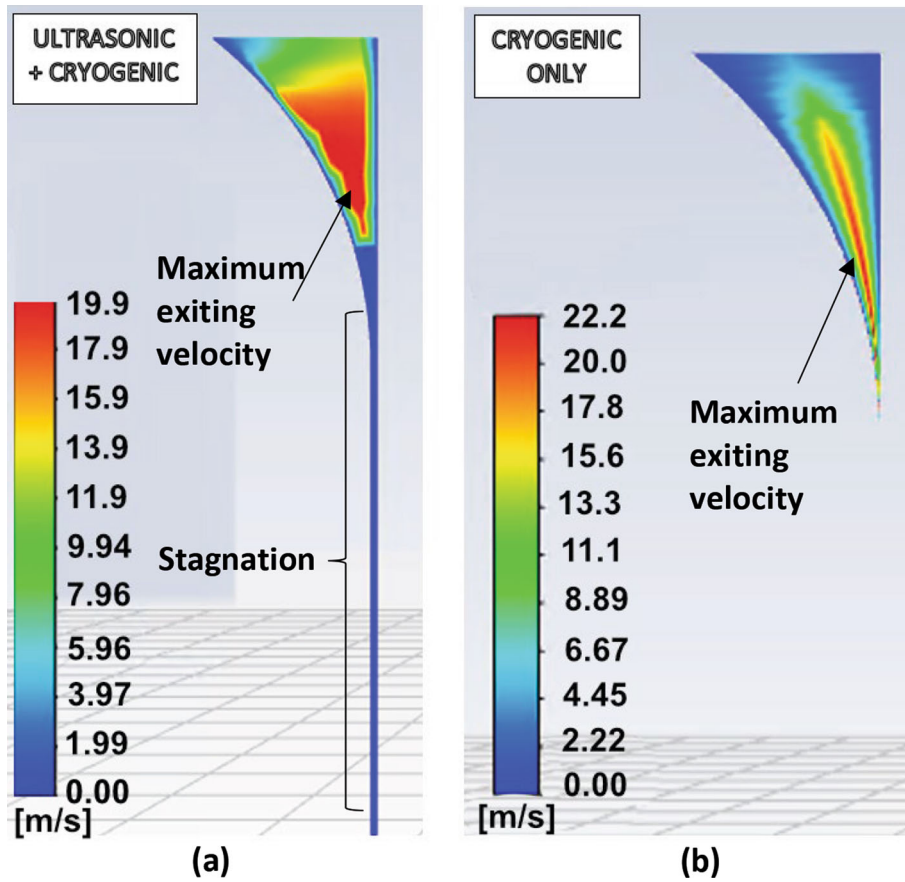


Figure 8 Velocity profiles of the tool–chip geometry for (a) combined machining and (b) cryogenic-only machining

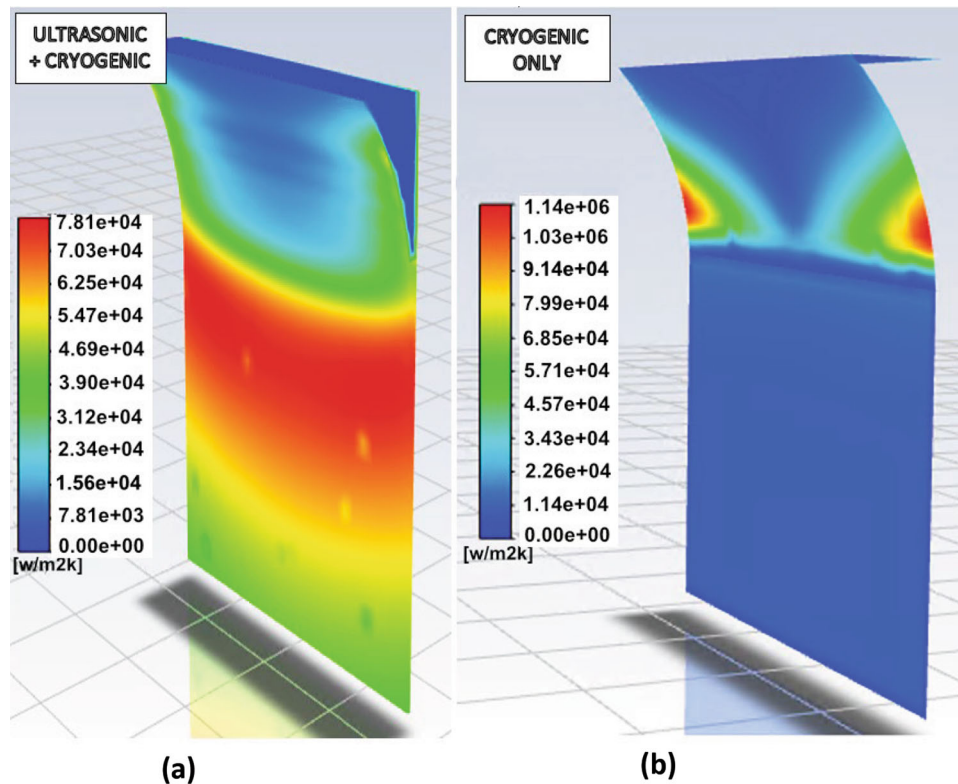


Figure 9 Convection coefficient profiles of the tool–chip geometry for (a) combined machining and (b) cryogenic-only machining

workpiece and thus allowing the fluid to flow into the gap and cool its surrounding. Another noticeable difference is the area affected by the cooling, where the cooled area in the case of the combined work is closer to the cutting edge than the cryogenic-only case. This implies a better cooling of the cutting edge itself and thus slows down the thermal softening of the tool at the cutting region. This finding may lead to reduced wear and a longer retention of a sharp cutting edge and improve the surface quality of the workpiece. In addition, some regions of the chip show a lower temperature in the cryogenic-only simulation, than their equivalent regions in the combined work; however, the main purpose of the cryogenic fluid appears to be the cooling of the tool, to slow down tool wear and improve surface quality of the workpiece (Ref 21).

Figure 8 shows the velocity profiles of the cryogenic fluid near the tool–chip interface. To satisfy the conservation of the mass flow rate, the cryogenic fluid in the cryogenic-only case exhibits a slightly higher velocity than the fluid in the combined case. Given the identical flow rates in both conditions, the larger exiting area for the fluid in the combined simulation results in the fluid leaves with a slower velocity of 19.9 m/s. It can also be observed that after a short period of time, the fluid reaches a stagnation in the gap for the case of the combined simulation, but in effect, this would not be the case due to the dynamic nature of the process. The motion of the chip, as well as the ultrasonic motion of the tool, would both lead to the draining of the fluid from the cutting zone, to be replaced with fresh incoming fluid from the cryogenic jet.

As expected, the cooling area covers a larger area of the cutting region, including the gap at the tool–chip interface due to the penetration of the cryogen in the combined case. While the maximum value of the convection coefficient is higher for

the case of the cryogenic-only, the distribution of the convection is very limited compared to the combined method, thus leading to an overall lower cooling effect in that case. This was confirmed by the lower cutting temperatures observed in Fig. 7.

Figure 9 shows the convection coefficient of the cryogenic coolant for the combined method and the cryogenic machining. The higher convection coefficient, shown in Fig. 9(a), in the case of cryogenic-only can be attributed to the higher velocity obtained for that case, which leads to a higher Reynolds number, Nusselt number and thus convection coefficient (Ref 22). As for the effect of the flow on the cooling abilities of the jet, the cryogenic fluid in the combined case exhibits a larger area of maximum velocity, compared to the thin strip of maximum velocity observed in the second case. The larger maximum-velocity region in the combined case indicates a higher turbulence of the fluid, indicated by the higher Reynolds number of the flow. This enhances its ability to absorb heat from its surroundings and cools down the material faster due to the transport eddies. The faster cooling rates in the combined case are supported by the plots of Fig. 9, which show the convection coefficient variation in the cutting region.

The average convection coefficient along the tool–chip interface was obtained from the CFD output and plotted, as shown in Fig. 9. These values were used as input to the FEM models to simulate the cutting of titanium Ti64 with cryogenic application as well as combined cryogenic and ultrasonic-assisted machining. The trends observed in Fig. 9 hold true for the curve obtained in Fig. 10. Once averaged out along the width of cut to be added to the 2D FEM, the maximum value obtained in the combined case ends up higher than the one for the cryogenic-only case, thus confirming the overall better cooling effect in the combined case.

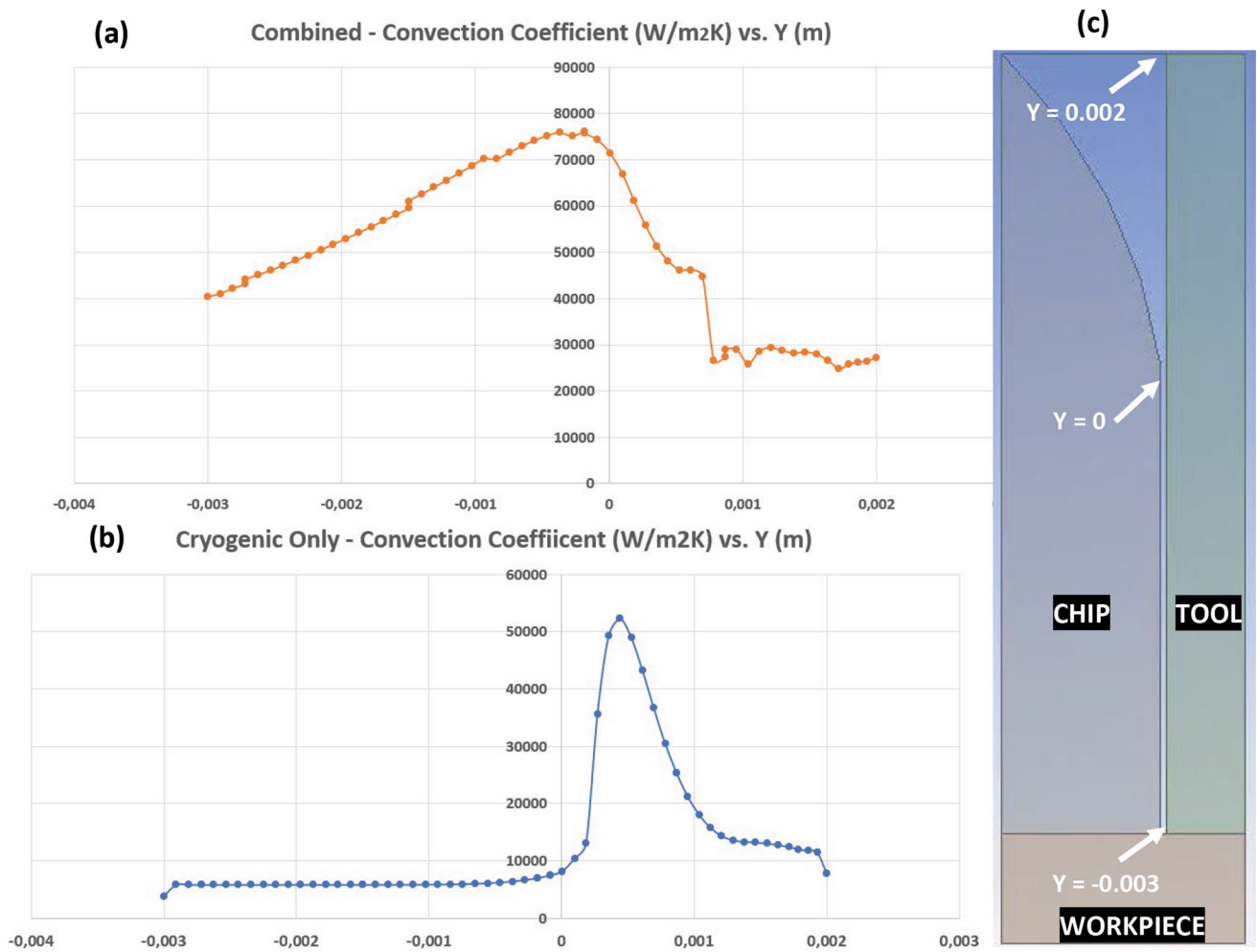


Figure 10 Convection coefficient variation along the tool for (a) combined machining and (b) cryogenic-only machining

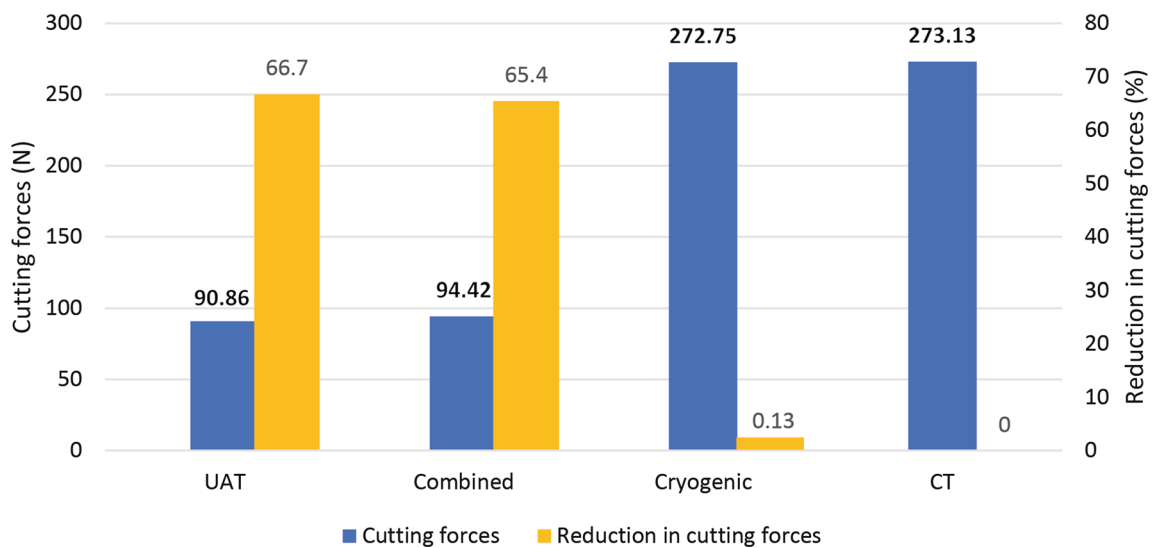


Figure 11 Average cutting forces and average reduction in cutting forces from simulations at 0.1 mm depth of cut and 7.2 m/min cutting speed

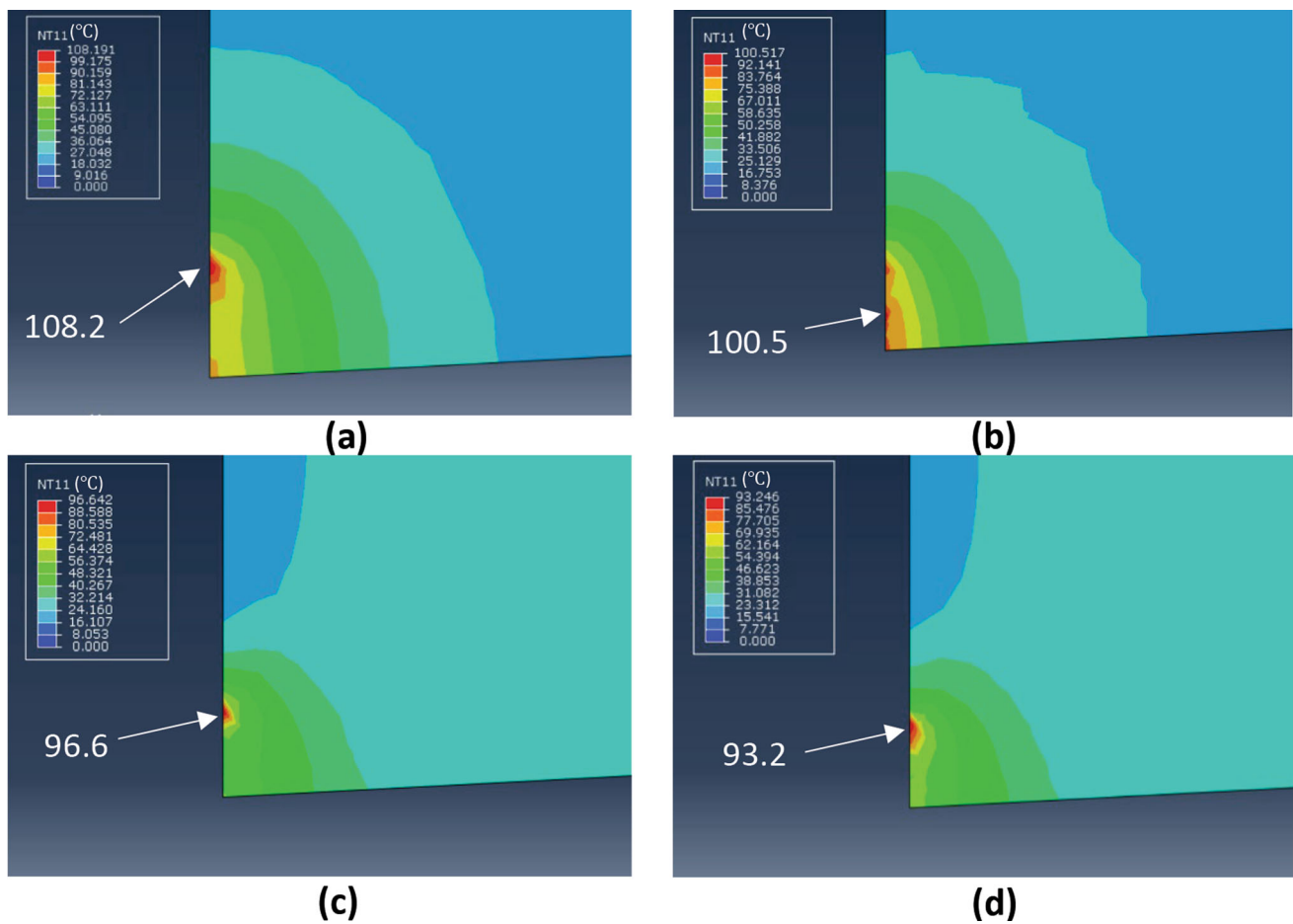


Figure 12 Tool temperature for (a) CT, (b) UAT, (c) CM and (d) combined method

4.1.2 FEM Results. The FEM simulations were conducted to simulate accurately the effect of the cryogenic coolant on the temperature of the tool, the cutting forces were also retrieved to have a better understanding of the mechanisms involved in the processes.

4.1.3 Cutting Forces. The cutting forces were retrieved from the simulations for dry cutting, UAT, cryogenic machining and the combined method. Figure 11 shows the average cutting forces and the reduction in the average cutting forces from simulations, respectively. The largest reduction in the cutting force was for UAT with a 67% reduction in cutting forces as compared to dry cutting. The combined method showed a similar reduction in the cutting forces with a 65% reduction in forces. The cryogenic, however, showed a slight decrease in the cutting forces with a decrease in 0.14%.

In UAT, the reduction in the cutting forces is due to separation which reduces the average cutting forces (Ref 5). Metal hardness typically increases with a decrease in temperature. The cryogenic turning reduces the cutting forces by mainly preserving the cutting edge of the tool, by reducing the cutting temperature and hardening the tool (Ref 21). The tool wear and deformation of the tool were not accounted for in these simulations since the tool was designed as a rigid body to study the heat transfer on the tool–chip interface. The lack of reduction in the cutting forces in the CM simulation confirms that the reduction in forces in CM experimentally is due to the

hardness retention of the tool, which is further discussed in Sect. 4.2.1. In the combined methods, separation is also present which explains the similarity in the results of the cutting forces.

4.1.4 Thermal Effect. Figure 12 shows the temperature of the cutting tool for the four tested processes. The highest tool temperature is observed for the UAT case, where the added vibrations introduce external energy to the cutting process. This added energy is added to the process and partially converted as thermal energy, increasing the cutting temperature and chip temperature, leading to an increase in the tool temperature by conduction between the tool and the hot chip (Ref 23). Additionally, the large instantaneous cutting speed also causes an increase in the cutting temperature (Ref 9).

The cryogenic and combined method resulted both in a decrease in tool temperature when compared to CT. The lowest tool temperature was observed for the combined method where the cryogenic coolant reduces the cutting temperature by entering the gap formed during the separation between the tool and the workpiece. The tool temperature was also reduced in the cryogenic machining. The applied coolant on the tool–chip interface reduces the cutting temperature significantly by convection. As mentioned previously, the cryogenic fluid has a higher convection coefficient for the cryogenic case alone in the zone above the tool–chip contact zone. However, in the combined method, the cryogenic coolant is allowed into the formed gap where the peak tool temperature is located, which

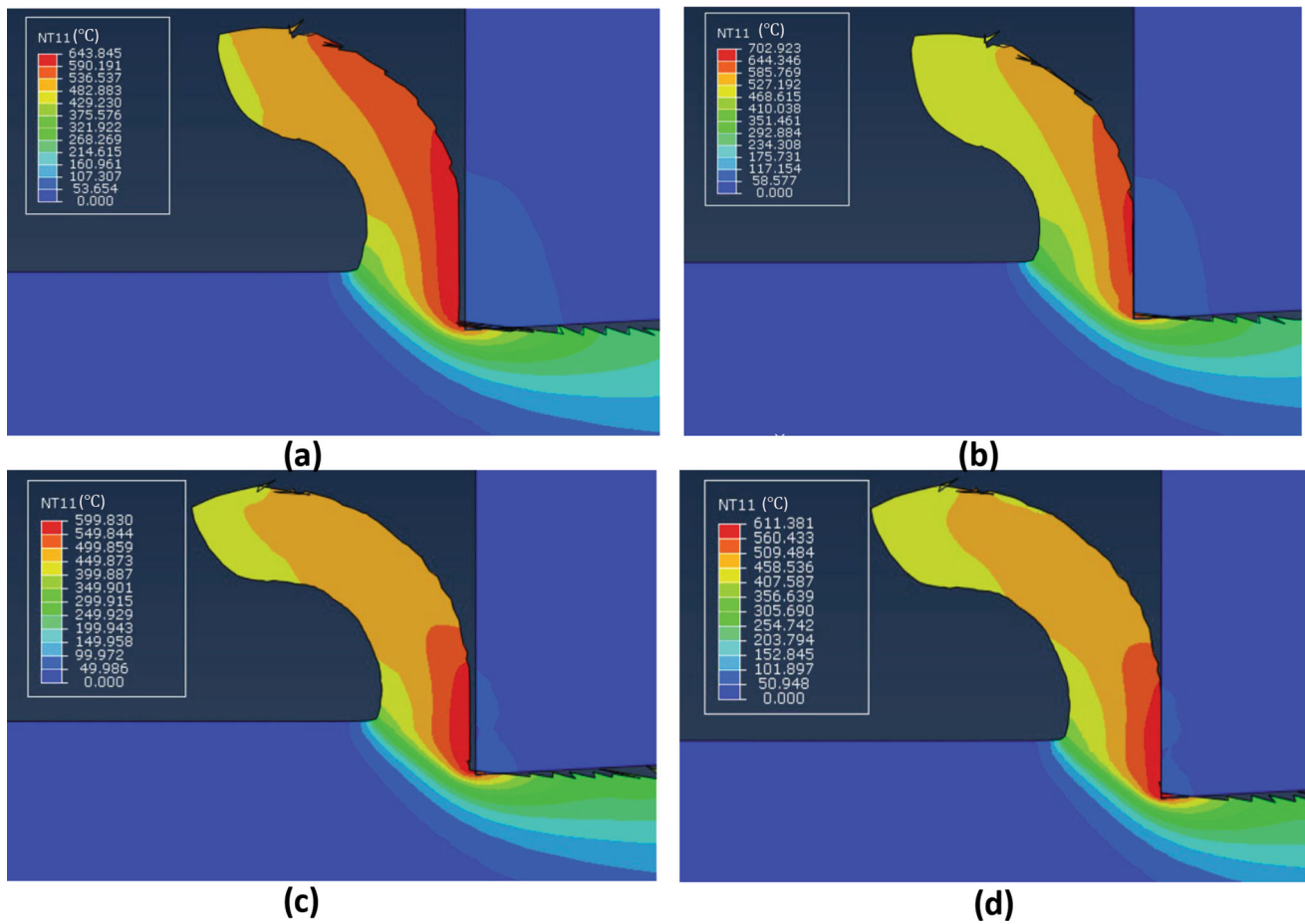


Figure 13 Chip temperature in (a), UAT separation, (b) UAT cutting, (c) combined separation and (d) combined cutting

allows a direct contact between the fluid and the area, reducing its temperature significantly.

The separation between the tool and the workpiece in the combined method allows the tool temperature to drop locally due to the conduction of the temperature within the tool without the addition of external heat from the chip. Moreover, the cooling of the section of the tool, above the tool–chip contact zone and the drop in the temperature in that area, creates a larger temperature gradient between that area and the peak tool temperature. The larger temperature gradient typically increases the heat transfer rate and the total heat being dissipated into the tool bulk. Therefore, the heat is dissipated at a higher rate in the combined method: by convection into the cryogenic fluid, by conduction into the tool in the vertical and horizontal direction. The tool temperature was retrieved from the FEM in this study since measuring the temperature at the tool–chip interface experimentally is beyond the scope of this work requiring the need of multiple thermocouples along the tool–chip interface.

It is also worth mentioning that the measurement of the temperature experimentally in the space between the nozzle and the tool–chip interface is very difficult. Therefore, a CFD model was used as explained in Sect. 2.1.

The reduction in tool temperature is usually related to reduced wear, which aligns well with our findings shown in Fig. 12. The low tool temperature in the combined method significantly reduces adhesion wear and diffusion since both

wear mechanisms are driven by high temperatures, as will be further discussed in Sect. 4.2.2 (Ref 24).

The chip temperature in UAT is larger than CT temperature as shown in Fig. 13. The high chip temperature has a softening effect on the titanium workpiece while the drop in tool temperature conserves the hardness of the tool. The larger relative tool hardness results in a reduction in the cutting forces in UAT. In the case of CM, the cryogenic coolant reduces the temperature of the chip and the workpiece, increasing the hardness of both simultaneously. However, the conservation of the edge of the tool combined with the difference in thermal conductivities of the workpiece and tool result in a larger hardening for the tool (Ref 17). However, in combined machining, the addition of cryogenic coolant lowers the chip temperature and the tool temperature further. The added cooling limits the softening effect of the added energy from the ultrasonic vibration, and consequently limits the reduction in forces. Although the tool is also cooled, the effect of the cryogenic coolant on the reduction in chip temperature is larger than the reduction in tool temperature. The chip temperature is reduced by 7.26% in the combined method when compared to UAT, while the tool temperature is reduced by 13.86%.

4.2 Experimental Results and Discussion

The cutting parameters explained in Sect. 3.1 were used in the experimentation to retrieve the cutting forces and analyze

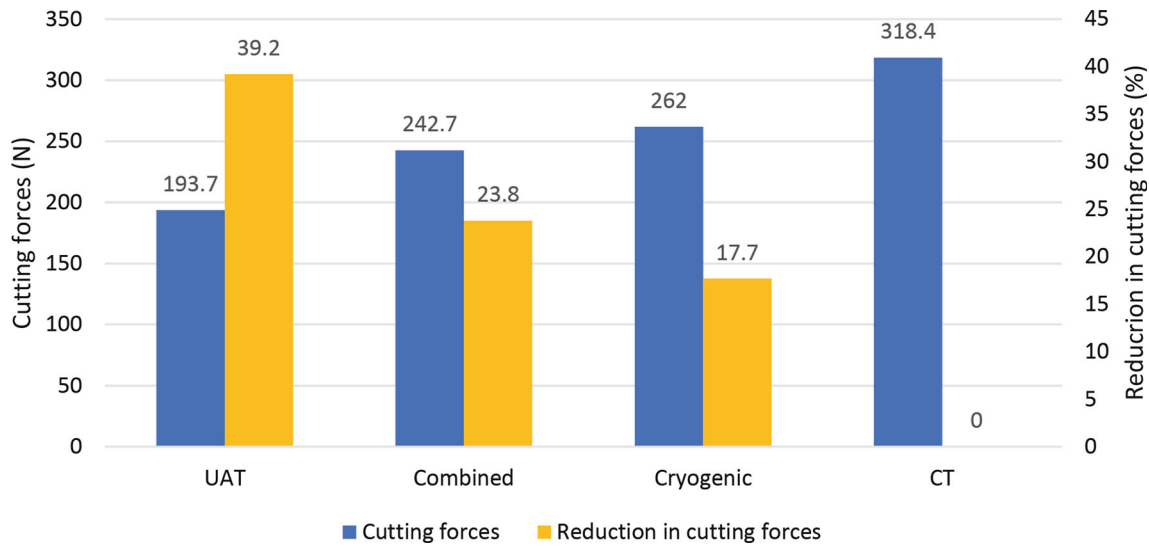


Figure 14 Average cutting forces and average reduction in cutting forces from experiments at 0.1 mm depth of cut and 7.2 m/min cutting speed.

the tool wear. The cutting forces were measured experimentally for ultrasonic, cryogenic and combined turning and were compared to the dry turning results for longitudinal turning. The tool wear was also studied for the different cutting processes to have a better understanding of the effect of combining both methods in one process.

4.2.1 Cutting Forces. Figure 14 shows the cutting forces for each turning process. The highest cutting forces were recorded, as expected, for the dry turning process. All the processes have shown a reduction in the cutting force. The largest decrease in the cutting forces was found in the UAT experiment, where a reduction of 39% of the cutting forces was found, as shown in Fig. 14. The CM also showed a significant reduction in the cutting forces by 17.7%. Combining the ultrasonic vibration with the cryogenic coolant reduced the cutting forces by 23.78%. The combined method resulted in an enhancement in the reduction of the cutting forces to the cryogenic method; however, it seemed to decrease the efficiency of the ultrasonic method in reducing the cutting forces.

Cryogenic machining is more effective in reducing the cutting forces at high cutting speeds when machining titanium alloys, since the reduction in the cutting and tool temperatures is needed more due to the large increase in chip temperature (Ref 25). The cryogenic coolant hardens the tool insert, conserving its edge which results in a reduction in forces. Furthermore, when a cryogenic coolant is applied, the decrease in workpiece toughness and ductility reduces the contact length between the tool and chip, and increases the shear plane angle, which results in a decrease in the cutting forces (Ref 26). At very low cutting speeds, the cutting temperatures and heat generation are low compared to those at higher cutting speeds. The reduced heat generation combined with the longer contact time between the cryogenic fluid and the workpiece before it evaporates results in a very pronounced cooling. Therefore, the required cutting forces will remain at a high level due to workpiece embrittlement since the machining zone is over-cooled at low cutting speeds (Ref 27). The low cutting speeds in these experiments reduced the effectiveness of the cryogenic coolant; however, the cutting parameters are convenient for ultrasonic turning, allowing the presence of separation since it

is only present at low cutting speeds (Ref 28). These conditions resulted in a high reduction in the cutting forces in the UAT experiments. In the literature, cryogenic machining at low cutting speeds showed a smaller reduction in cutting forces compared to machining at high cutting speeds (Ref 29). Further research is required to investigate the effect of the combined method (ultrasonic and cryogenic) at higher cutting speeds and compare it to lower cutting speeds.

When combining CM and UAT, the previously discussed reduction in chip temperature results in limiting the softening effect due to the added energy from the vibration of the tool which increases the cutting forces when compared to UAT. However, UAT also reduces the average cutting forces due to the separation which interrupts the cutting process periodically registering zero cutting forces (Ref 30). This phenomenon is applicable in the combined method, where separation is present, reducing the average cutting forces, which explains the reduction of forces in the combined method in these experiments.

The FEM cutting forces are not comparable to the experimental cutting forces since the FEM was performed in a 2D orthogonal cutting, as mentioned in Sect. 2.2.1. However, the trends in the reduction of the cutting forces in the FEM simulations and the experiments are similar. No wear model was introduced in the FEM model in this study; therefore, the forces will not reveal the progress of tool wear or the tool hardening in cases where the cryogenic fluid is applied. Since the FEM model was validated previously (see Sect. 2.2.1), the output should reasonably replicate the trends with the addition of variable convection and an oscillating tool.

The literature suggests that using a liquid nitrogen (LN₂)-based cryogenic coolant results in a lower friction coefficient than in dry sliding (Ref 31). No previous study investigating the effect of the friction coefficient was found for the carbon-based cryogenic fluid which was used in this work. Therefore, the FEM model used in this work did not account for variations in the friction coefficient. This can explain the reason behind the smaller reduction in the cutting forces in the FEM model compared to the experiments, when the cryogenic fluid is applied. The effect of the carbon-based cryogenic machining on

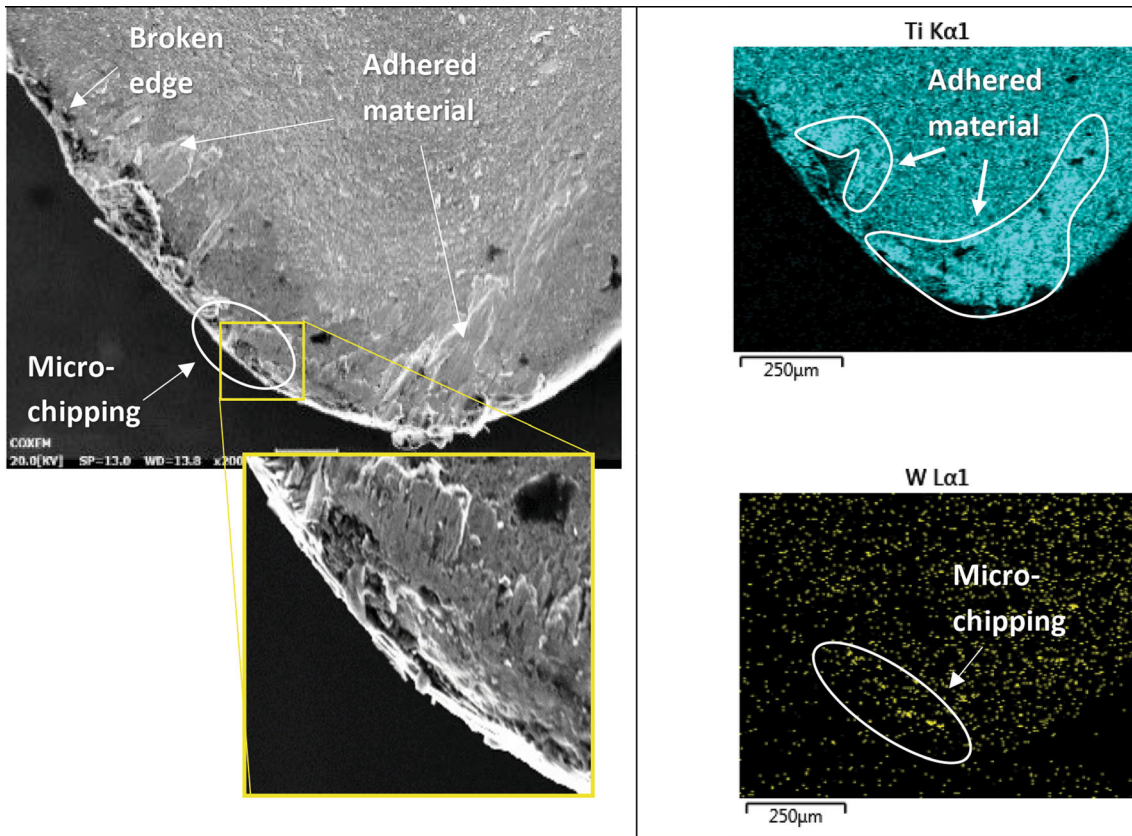


Figure 15 Tool wear in CT on the rake face

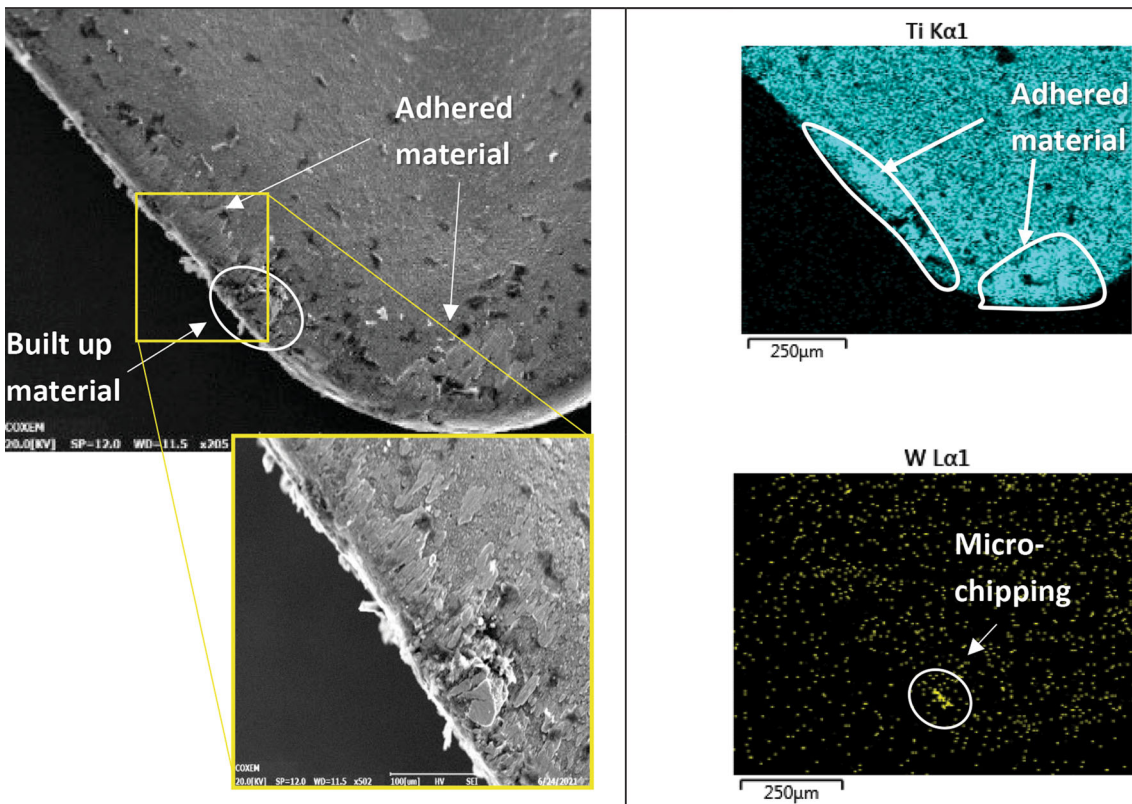


Figure 16 Tool wear in UAT on the rake face

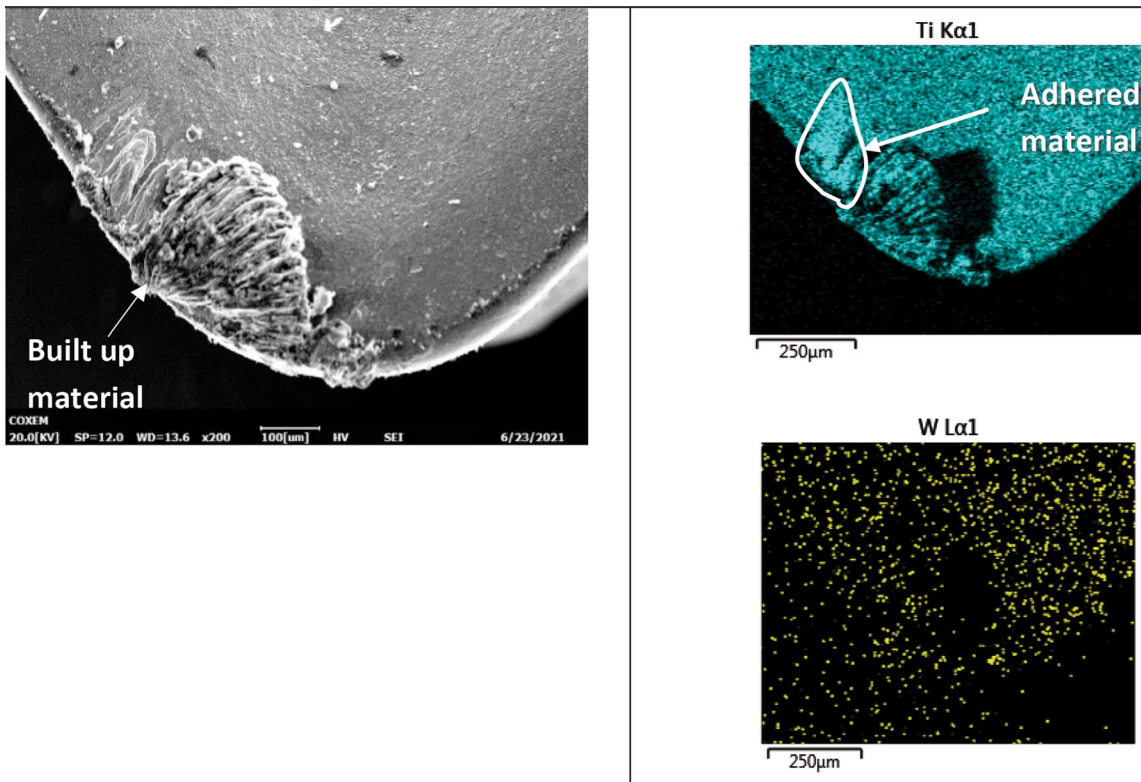


Figure 17 Tool wear in CM on the rake face

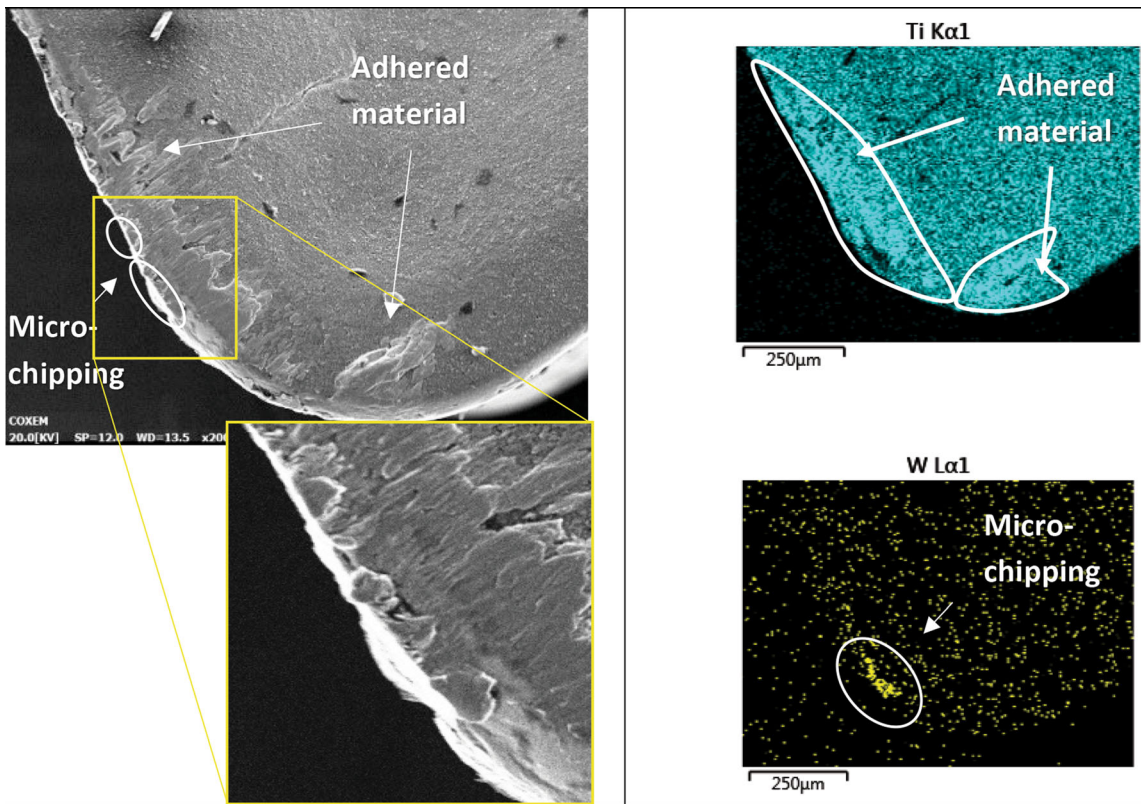


Figure 18 Tool wear in combined method on rake face

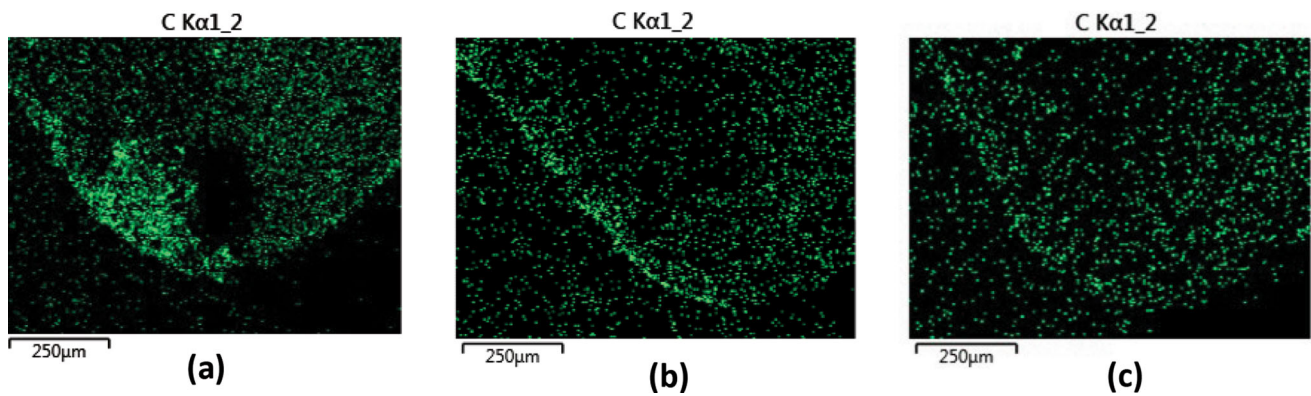


Figure 19 Carbon atoms on the rake face of the tool in (a) CM, (b) UAT and (c) combined method

the friction coefficient is an interesting topic to investigate in future work and would increase the precision of the FEM model when cryogenic fluid is used.

4.2.2 Tool Wear. The evaluation of the tool wear was conducted using confocal microscope, scanning electron microscope (SEM) and energy-dispersive spectroscopy (EDS) analysis.

When turning titanium with carbide tool inserts, adhesion wear and diffusion wear are generally dominant (Ref 32). The low thermal conductivity of the titanium alloy commonly results in a high cutting temperature which is the driving factor behind adhesion and diffusion wear. Figure 15, 16, 17 and 18 shows the SEM and EDS images of the rake of the tools used for the longitudinal turning of titanium alloy. The SEM image of the tool used in CT, shown in Fig. 15, shows large strains of adhesion on the workpiece. The adhered material on the workpiece tends to break off regularly from the workpiece creating micro-chipping on the edge of the tool as shown in Fig. 15, where more adhered material can fill the created micro-chips. The exposed tungsten reveals possible areas where the tool incurred micro-chipping.

In UAT, shown in Fig. 16, the adhesion wear and the micro-chipping are substantially reduced. The addition of ultrasonic vibrations to the motion of the tool created a separation between the tool and the workpiece. Therefore, the decrease in contact duration decreases adhesion wear. In addition, the reduction in the cutting forces reduces the pressure exerted on the tool edge and hence the micro-chipping, as shown in Fig. 16. The addition of the cryogenic coolant also reduces the adhesion and consequently the micro-chipping of the tool, as shown in Fig. 17 for the CM experiment. This reduction in wear may be caused by the combination of the reduced cutting forces and the harder tool edge due to the heat transferred from the tool to the cryogenic fluid.

When combining the ultrasonic vibrations with the cryogenic cooling, a mixed effect can be observed, as shown in Fig. 18. The adhesion wear is reduced remarkably when compared to CT and cryogenic machining and is like the adhesion wear found in UAT. However, micro-chipping is increased when compared to each method separately. The increase in micro-chipping is due to the increase in the hardness of the workpiece which is caused by the reduction in chip temperature from the cooling. The increase in hardness causes

an increase in the cutting forces in the combined method compared to UAT. The higher cutting forces, coupled with the impact caused by the periodic separation and contact between the tool and the workpiece, could result in the micro-chipping on the edge of the tool where the tungsten can be seen in the EDS image. The separation is positively affecting the tool wear in the combined method, where the intermittent contact between the tool and the workpiece reduces the adhesion wear similarly to UAT, and the flowing coolant acts as a lubricant, creating a layer of lubrication on the tool–chip interface which further decreases adhesion wear.

Diffusion wear when machining titanium is promoted by the high cutting temperature and contact between the tool and the chip (Ref 33). Figure 19 shows the carbon elements on the rake face of the tool for UAT, CM and the combined method. When cutting titanium, carbon atoms in the carbide tool are separated from the tungsten atoms (Ref 34). The constant contact with the chip which has a high temperature promotes the diffusion of the carbon atoms to the surface of the tool and are mixed with the adhered titanium on the surface (Ref 26). The limited contact in UAT between the tool and the chip decreases the rate of diffusion of the carbon atoms which results in a low concentration of carbon atoms on the tool's edge, as shown in Fig. 19. In cryogenic machining, the reduced tool temperature also decreases diffusion wear. However, the effect of the cryogenic cooling on the diffusion wear for low cutting speeds is limited since the cutting temperature is lower than the temperature at high cutting speeds.

For the combined method, the EDS results show a lower carbon level. The combination of ultrasonic vibrations with the cryogenic coolant decreases immensely diffusion wear by decreasing the chip temperature and decreasing the contact time between the tool and the chip. The effect of UAT and CM on diffusion wear is complementary, where both methods decrease the diffusion wear in separate and uncontradictory mechanisms. The effect of cryogenic turning is thermal, in reducing the chip temperature, while the ultrasonic turning is mechanical, in reducing contact time.

Figure 20 shows the optical images of the tool's surface for the four experiments and Fig. 21 shows the confocal images of the surface topography. The results in Fig. 20 validate the analysis from the SEM and EDS. Adhesion wear is present in all the experiments with a higher concentration in CT. The edge

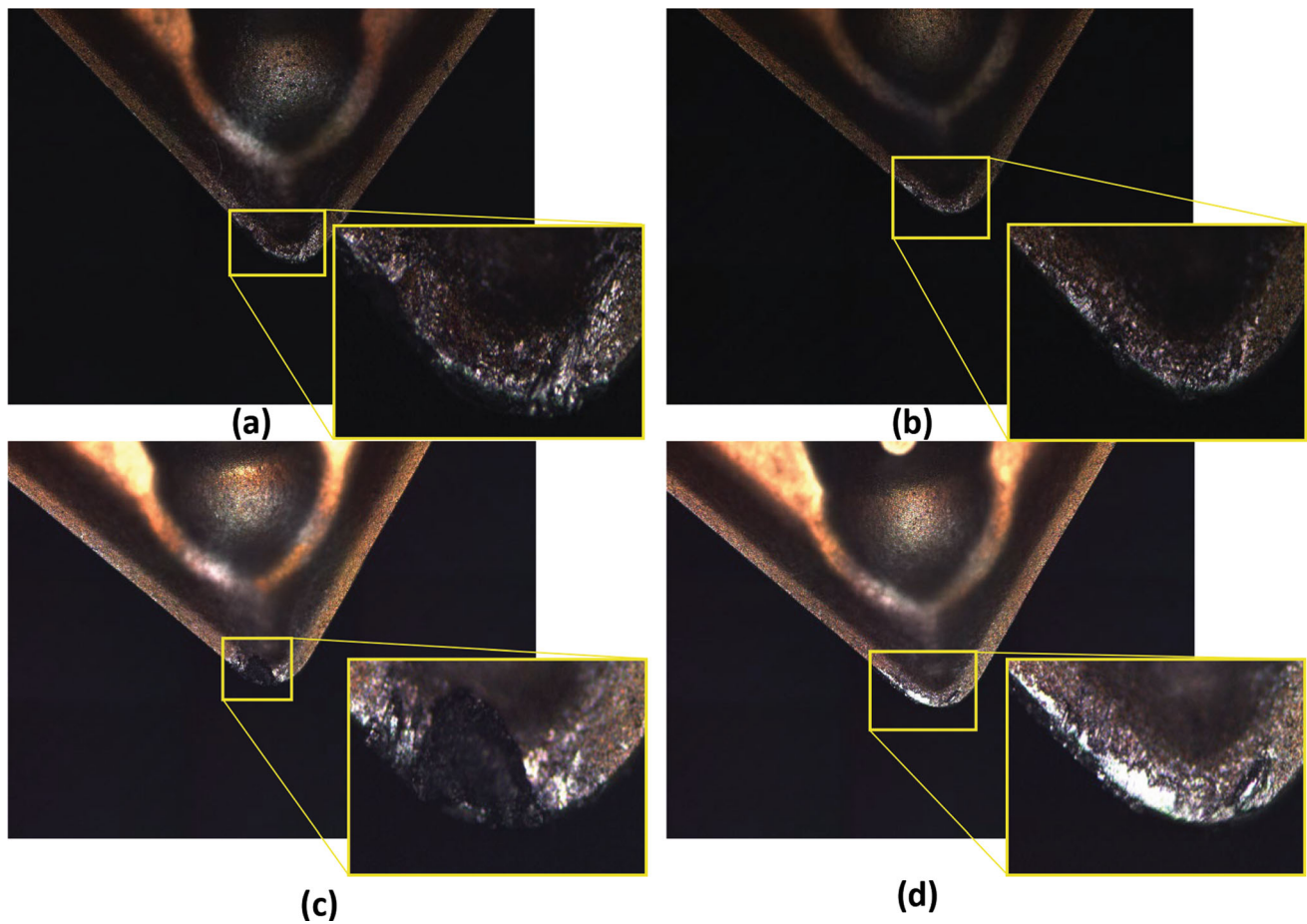


Figure 20 Optical images of tool wear on the rake face in (a) CT, (b) UAT, (c) CM and (d) combined method

is conserved in the combined method with a reduction in adhesion wear. In Fig. 20(b) and (d) for the UAT and the combined method, the adhesion wear is comparable, with a slighter reduction in adhesion wear in the UAT method. In Fig. 20(c), the buildup of material in CM is observed. This buildup of material may break off the cutting tool edge and create micro-chips on the tool's edge. Unstable built-up edge (BUE) is known to be detrimental for tools. In the combined method, the buildup of material is minimal, which would result in a greater reduction in micro-chipping on the tool's edge as the cutting time increases extending the tool's life.

The buildup of material is validated by the confocal images of surface topography, where the largest peak can be found for CM, of approximately 60 microns above the tool's edge. Furthermore, the buildup of material is reduced immensely in the UAT and combined method, while micro-chipping is also reduced in the combined method, confirming the added benefits from the combination of the ultrasonic vibrations and the cryogenic coolant.

Abrasion wear is the dominant wear on the flank side of the carbide tool when turning titanium (Ref 32). The high friction between the tool and the workpiece causes abrasion on the tool, which when combined with the adhesion and diffusion increases the flank wear. Figure 22 shows the SEM and EDS results for the flank wear of the inserts used in the experiments. The largest flank wear is observed for CT, while a reduction in concentration of titanium atoms and adhered material is found for CM and UAT. Each method reduces wear in a different

mechanism. In UAT, the reduction in flank wear is minimal due to the constant friction between the tool and the workpiece since the separation in the one directional vibration occurs only on the rake face. The addition of vibration will not reduce friction since the tool is always in contact along the flank side due to the motion of the tool; however, the intermittent cutting and flow of chips result in an overall decrease in flank wear. In CM, the addition of the coolant reduces the friction between the tool and the workpiece therefore reduces the flank wear, specifically abrasion and adhesion (Ref 35).

In the combined method, shown in Fig. 22(d), the same abrasion marks as the UAT method can be observed. The abrasion is caused by the friction of the tool with the workpiece as the tool insert is vibrating in a parallel motion to the flank side while staying in contact with the workpiece. Furthermore, the increase in the hardness of the tool can promote abrasion in the combined method due to increased hardness resulting from the coolant. Also, the longer strains of titanium on the flank of the tool confirm that the adhesion wear is being promoted by the vibration of the tool, since the strains are longer in the UAT and the combined method than the ones found in CM. The addition of the cryogenic coolant reduces the adhesion wear from CT; however, the effect of combining the methods on tool wear is less significant on the flank side of the tool when compared to its effect on the rake face where the separation is. As mentioned earlier, increasing the cutting speed would enhance the efficiency of the CM method in reducing wear and decrease the efficiency of the UAT method, which may result in

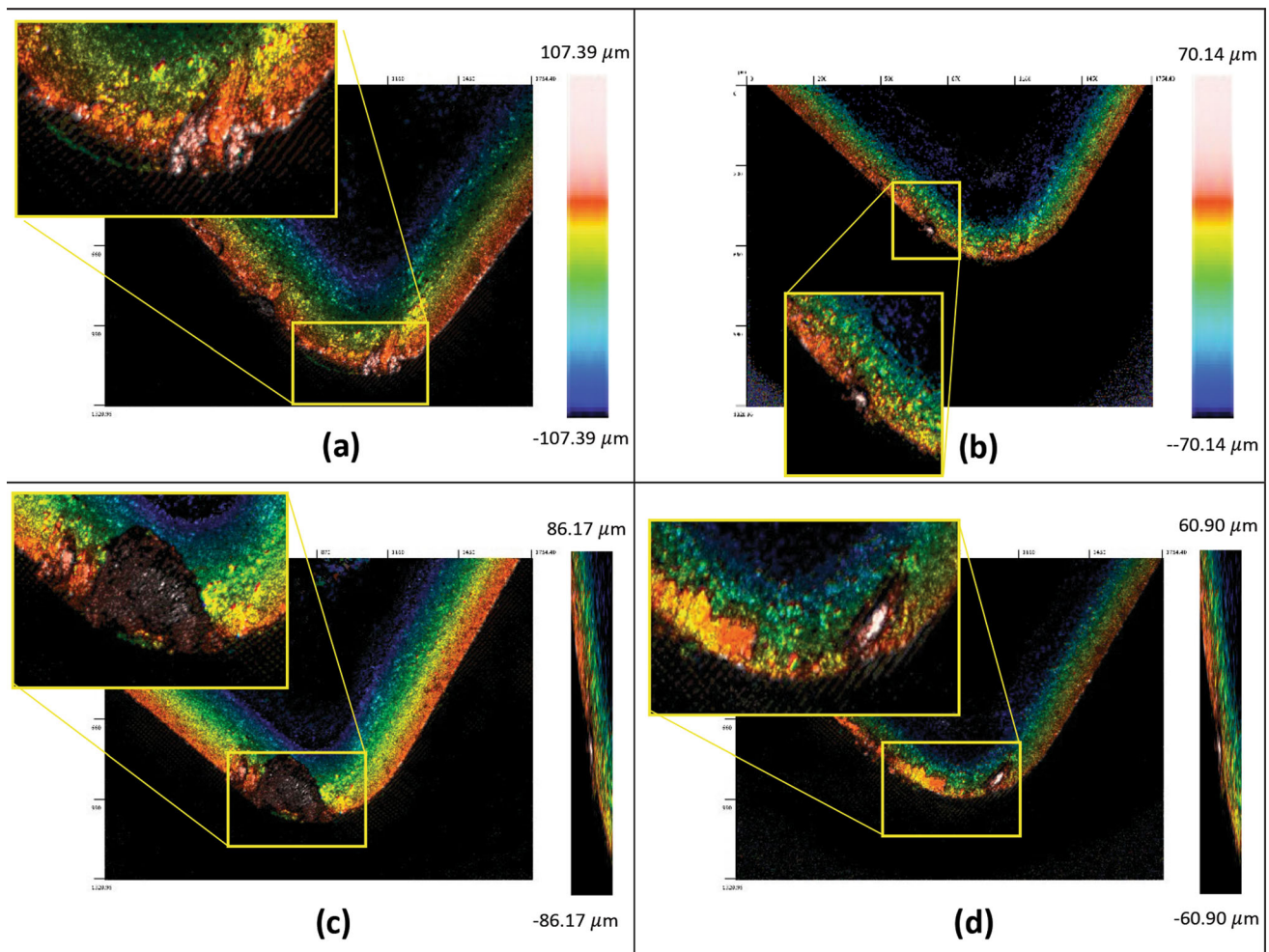


Figure 21 Confocal images of surface topography on the rake face of the tool in (a) CT, (b) UAT, (c) CM and (d) combined method

an advantage in combining the methods as compared to using each separately.

5. Conclusions

This research investigated the combination of ultrasonic vibration and cryogenic machining where UAT and CT are combined in a single process using CFD, FEM and experimentation. The simulation results were used to better understand the physics behind each of the processes and support the analysis of tool wear using the temperature results.

It was found that combining UAT with CM resulted in a significant decrease in cutting forces and reduction in tool wear when compared to CT when machining Ti-6Al-4V.

The literature lacks a study for the combined effect of ultrasonic-assisted turning and cryogenic machining. The variable convection coefficient of the cryogenic fluid was retrieved from the CFD and used as input in an FEM model. The variable convection coefficient was applied along the rake

face of the tool and the chip. The ultrasonic vibrations were added to the tool to simulate the combined method and investigate the thermal effect of the process on the tool and chip temperature. Experiments were conducted afterward to retrieve the cutting forces and analyze the tool wear. The FEM temperature profile and convection coefficient, in addition to microscopy were used to analyze tool wear.

The UAT had the largest decrease in the cutting forces. The combined method had the second largest decrease, whereas the cryogenic machining had the least reduction in cutting forces when compared to dry cutting:

- The added energy in the UAT method, which was partly transformed into thermal energy increased the chip temperature, softening the titanium alloy. This softening effect resulted in lower cutting forces.
- The addition of the cryogenic fluid had a cooling effect on the formed chip, which hardened the material, resulting in an increase in the cutting forces when compared to the UAT method.

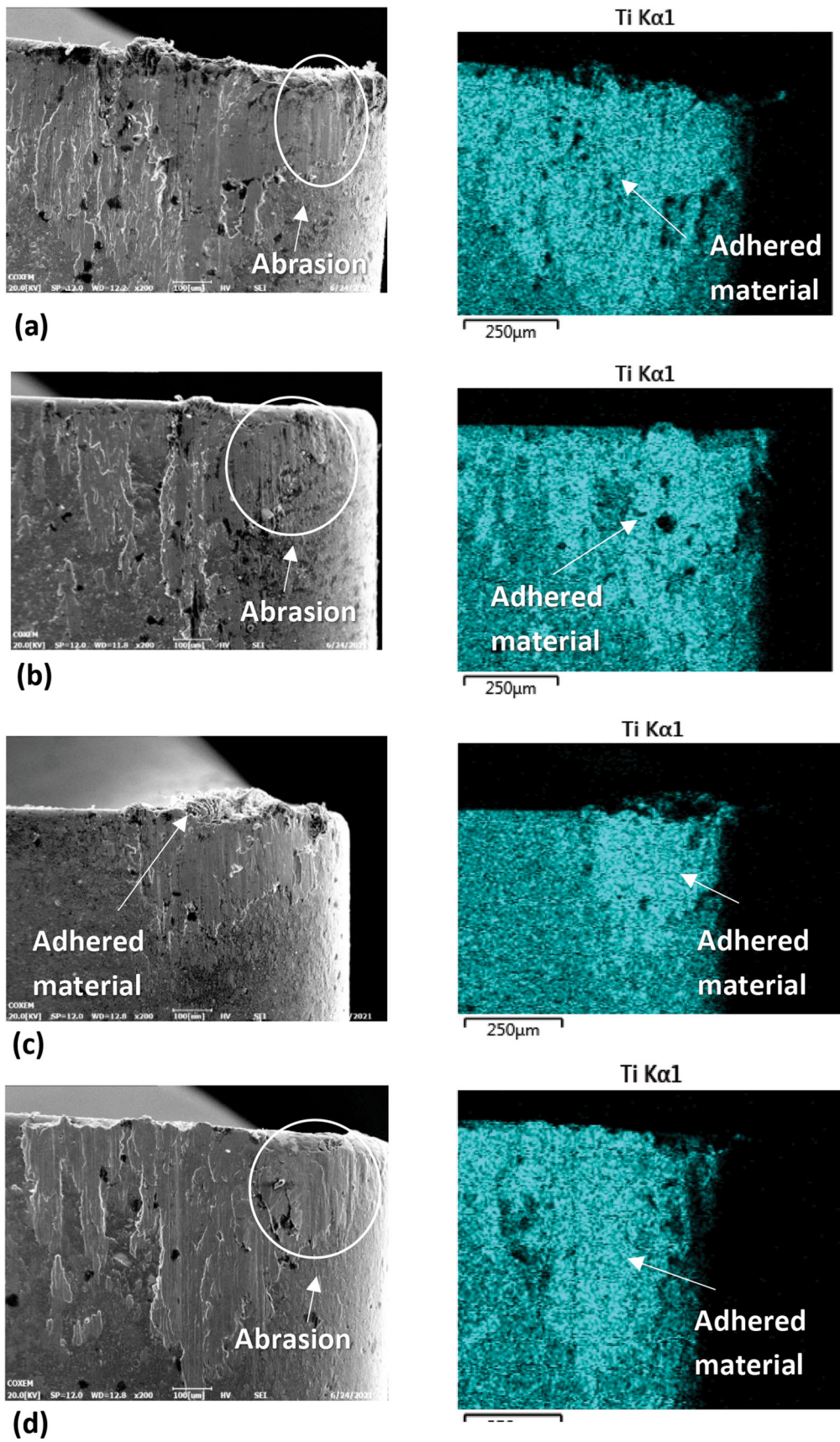


Figure 22 SEM and EDS images of flank wear in (a) CT, (b) UAT, (c) CM and (d) combined method

The combined method showed the most significant reduction of tool wear, followed by the UAT method, then the cryogenic method when compared to dry cutting:

- The high convection in the combined method resulted in a low temperature on the tool's rake face, which resulted in a reduction of wear.
- Lowering the titanium's temperature with cryogenic is associated with an increase in hardness; therefore, the addition of the cryogenic fluid to the ultrasonic method cooled and consequently hardened the titanium alloy. This may explain the increase in the cutting forces when compared to the ultrasonic method. The higher cutting forces, added to the impact due to the separation, lead to the observation of micro-chipping.

Recommended future work could take this study further by adding a deformable tool and a wear model to accommodate for the effect of wear on forces when different machining methods are used. To facilitate possible future industrial applications, future research could look into varying and optimizing the parameters of the cryogenic coolant such as the pressure and the nozzle position.

The experimental measurement of the temperature at the tool-chip interface would be interesting to investigate in future work. This may require a special tool with multiple thermocouples. Future work could also focus on the productivity aspect where different tools and parameters can be optimized for increasing productivity.

Funding

No funding was received to assist with the preparation of this manuscript.

Conflict of interest

The authors declare that they have no conflict of interest.

References

1. P. Olander and J. Heinrichs, Initiation and Propagation of Tool Wear in Turning of Titanium Alloys—Evaluated in Successive Sliding Wear Test, *Wear*, 2019, **426–427**, p 1658-1666
2. H. Abdel-Aal, M. Nouari and M. El Mansori, Influence of Thermal Conductivity on Wear when Machining Titanium Alloys, *Tribol. Int.*, 2009, **42**, p 359-372
3. G. Dhurian, R. Singh and A. Batish, Predictive Modeling of Surface Roughness in Ultrasonic Machining of Cryogenic Treated Ti-6Al-4V, *Int. J. Comput. Aided Eng. Softw.*, 2016, **33**(8), p 2377-2394
4. J. Zhang and D. Wang, Investigations of Tangential Ultrasonic Vibration Turning of Ti6Al4V using Finite Element Method, *Int. J. Mater. Form.*, 2019, **12**, p 257-267
5. S. Patil, S. Joshi, A. Tewari and S.S. Joshi, Modelling and Simulation of Effect of Ultrasonic Vibrations on Machining of Ti6Al4V, *Ultrasonics*, 2013, **54**, p 694-705
6. V. Sharma and P.M. Pandey, Recent Advances in Ultrasonic Assisted Turning: A Step Towards Sustainability, *Cogent Eng.*, 2016, **3**, p 1222776
7. M.A. Sofuoglu, F.H. Çakır, S. Gorgen, S. Orak and M.C. Kushan, Numerical Investigation of Hot Ultrasonic Assisted Turning of Aviation Alloys, *J. Braz. Soc. Mech. Sci. Eng.*, 2018, **40**(3), p 1–12
8. X. Zhang, Z. Peng and L. Liu, A Transient Cutting Temperature Prediction Model for High-Speed Ultrasonic Vibration Turning, *J. Manuf.*, 2022, **83**, p 257–269
9. B.D. Jerold and M.P. Kumar, The Influence of Cryogenic Coolants in Machining of Ti-6Al-4V, *J. Manuf. Sci. Eng.*, 2013, **135**(3), p 031005.
10. M.I. Sadik and S. Isakson, The Role of PVD Coating and Coolant Nature in Wear Development Tool Performance in Cryogenic and Wet Milling of Ti64, *Wear*, 2017, **386–387**, p 204-210
11. A. Bordin, S. Bruschi, A. Ghiotti and P. Bariani, Analysis of Tool Wear in Cryogenic Machining of Additive Manufactured Ti6Al4V Alloy, *Wear*, 2015, **328–329**, p 88-99
12. A. Damir, A. Sadek and H. Attia, Characterization of Machinability and Environmental Impact of Cryogenic Turning of Ti-6Al-4V, *Procedia CIRP*, 2018, **69**, p 893–898
13. J. Airao, C.K. Nirala, L.N.L. de Lacalle and N. Khanaa, Tool Wear Analysis during Ultrasonic Assisted Turning of Nimonic-90 under Dry and Wet Conditions, *Metals*, 2021, **11**(8), p 1253
14. S. Manel and S. Kumar, Heat Generation and Temperature in Orthogonal Machining, *Int. J. Sci. Eng. Res.*, 2017, **8**(2), p 31–33
15. ANSYS, ANSYS Fluent Theory Guide, ANSYS, Inc., Canonsburg, 2013
16. C. Salame, R. Bejjani and P. Marimuthu, A Better Understanding of Cryogenic Machining Using CFD and FEM Simulation, in *52nd CIRP Conference on Manufacturing Systems*, Vol. 81, 2019, p. 1071-1076
17. R. Bejjani, C. Salame, A better understanding of the cryogenic environment and the effect of nozzle location on the machinability of low carbon steel, *J. Manuf. Process.*, 2022, **74**, p 544-556
18. M. Smith, ABAQUS/Standard User's Manual, Version 6.9, *Dassault Systèmes Simulia Corp.*, 2009
19. K.V. Sekar and M.P. Kumar, Finite element simulations of Ti6Al4V titanium alloy machining to assess material model parameters of the Johnson–Cook constitutive equation, *J. Braz. Soc. Mech. Sci. Eng.*, 2011, **33**, p 203–211
20. K. Hu, S.-L. Lo, H. Wu and S. To, Study on Influence of Ultrasonic Vibration on the Ultra-Precision Turning of Ti6Al4V Alloy Based on Simulation and Experiment, *IEEE Access*, 2019, **7**, p 33640–33651
21. S. Sun, M. Brandt and M. Dargusch, Machining Ti-6Al-4V Alloy with Cryogenic Compressed Air Cooling, *Int. J. Mach. Tools Manuf.*, 2010, **50**(11), p 933–942
22. B. Lindeman and T. Shedd, Comparison of Empirical Correlations and a Two-Equation Predictive Model for Heat Transfer to Arbitrary Arrays of Single-Phase Impinging Jets, *Int. J. Heat Mass Transf.*, 2013, **66**(2), p 772–780
23. F. Wang, J. Zhao, Z. Li and A. Li, Coated Carbide Tool Failure Analysis in High-Speed Intermittent Cutting Process Based on Finite Element Method, *Int. J. Adv. Manuf. Technol.*, 2016, **83**, p 805–813
24. CIRP Encyclopedia of Production Engineering, 2014
25. D. Bai, J. Sun, W. Chen and T. Wang, Wear Mechanisms of WC/Co Tools when Machining High-Strength Titanium Alloy TB6 (Ti-10V-2Fe-3Al), *Int. J. Adv. Manuf. Technol.*, 2017, **90**, p 2863–2874
26. S.Y. Hong and Z. Zhao, Thermal Aspects, Material Considerations and Cooling Strategies, *Clean Technol. Environ. Policy*, 1999, **1**(2), p 107–116
27. N. Khanna and C. Agrawal, Materials Forming, *Machining and Tribology*, Springer, Berlin, 2019, p 183–205
28. M. Khajehzadeh, O. Boostanipour and M.R. Razfar, Finite Element Simulation and Experimental Investigation of Residual Stresses in Ultrasonic Assisted Turning, *Ultrasonics*, 2020, **108**, p 106208
29. C. Agrawal, J. Wadhwa, A. Pitroda, C.I. Prunco, M. Sarikaya and N. Khanna, Comprehensive Analysis of Tool Wear, Tool Life, Surface Roughness, Costing and Carbon Emissions in Turning Ti-6Al-4V Titanium Alloy: Cryogenic Versus Wet Machining, *Tribol. Int.*, 2021, **153**, p 106597
30. M. Lotfi and S. Amini, FE Simulation of Linear and Elliptical Ultrasonic Vibrations in Turning of Inconel 718, *J. Process Mech. Eng.*, 2017, **232**, p 438–448
31. S.Y. Hong, Y. Ding and J. Jeong, Experimental Evaluation of Friction Coefficient and Liquid Nitrogen Lubrication Effect in Cryogenic Machining, *Mach. Sci. Technol.*, 2002, **6**(2), p 235–250
32. R. Bejjani, M. Balazinsk, H. Attia and P. Plamondon, Chip Formation and Microstructure Evolution in the Adiabatic Shear Band when Machining Titanium Metal Matrix Composites, *Int. J. Mach. Tools Manuf.*, 2016, **109**, p 137–146

33. R. Bejjani, E. Bamford, S. Cedergren, A. Archenti and A. Rashid, Variations in the Surface Integrity of Ti6Al-4V by Combinations of Additive and Subtractive Manufacturing Processes, *Materials*, 2020, **13**, p 1825
34. D.J. Schrock, D. Kang, T.R. Bieler and P. Kwon, Phase Dependent Tool Wear in Turning Ti-6Al-4V Using Polycrystalline Diamond and Carbide Inserts, *J. Manuf. Sci. Eng.*, 2014, 136(4), p 041018
35. C. Courbon, F. Pusavec, F. Dumont, J. Rech and J. Kopac, Tribological Behaviour of Ti6Al4V and Inconel718 under Dry and Cryogenic Conditions—Application to the Context of Machining with Carbide Tools, *Tribol. Int.*, 2013, 66, p 72-82

Publisher's Note Springer Nature remains neutral with regard to jurisdictional claims in published maps and institutional affiliations.

Springer Nature or its licensor (e.g. a society or other partner) holds exclusive rights to this article under a publishing agreement with the author(s) or other rightsholder(s); author self-archiving of the accepted manuscript version of this article is solely governed by the terms of such publishing agreement and applicable law.